Title

Squash ensures Spindle-E–dependent heterotypic ping-pong amplification of piRNAs in the *Drosophila* ovary

Authors

Xin Xu[1], Taichiro Iki[1], Shinichi Kawaguchi[1, *], Toshie Kai[1, 2, *]

Affiliations

[1] Graduate School of Frontier Biosciences, The University of Osaka, Osaka 565-0871, Japan

[2] Graduate School of Biostudies, Kyoto University, Kyoto, Japan.

* Corresponding author

E-mail:

Toshie Kai: kai.toshie.fbs@osaka-u.ac.jp, kai.toshie.2w@kyoto-u.ac.jp

Shinichi Kawaguchi: kawaguchi.shinichi.fbs@osaka-u.ac.jp

Key words

piRNA, transposon, nuage, *Drosophila*, Squash, Spindle-E.

Abstract

The PIWI-interacting RNA (piRNA) pathway plays a crucial role in repressing mobile transposable elements (TEs) and protecting the integrity of the heritable genome in animal gonads. In the *Drosophila* ovary, piRNAs are produced in a membrane-less organelle called nuage, in which many piRNA factors are localized. Among them, Squash (Squ) has also been identified as a key component in piRNA-directed TE silencing. However, its molecular function remains largely unknown. Here, we demonstrate that loss of Squ leads to defective piRNA biogenesis, which is associated with the abnormal accumulation of precursor transcripts and the specific destabilization of Ago3, a member of the PIWI-family proteins. Reducing Ago3 results in enhanced homotypic piRNA amplification mediated by Aub itself, rather than the heterotypic ping-pong amplification between Aub and Ago3. Additionally, we demonstrate that Squ is a functional cofactor of the RNA helicase, Spindle-E (Spn-E), which plays a vital role in piRNA biogenesis. Point mutations that abrogate the interaction between Squ and Spn-E result in TE de-repression and defective precursor processing, suggesting that Squ works with Spn-E to ensure the proper piRNA biogenesis. These results identify Squ as a critical factor for Spn-E–dependent heterotypic ping-pong amplification of piRNAs in the *Drosophila* ovary.

Introduction

Transposable elements (TEs) are mobile genetic elements that can replicate and insert into new genomic locations, present in most eukaryotic organisms (Wells and Feschotte, 2020). Although TEs have contributed substantially to the evolution of genomes, their uncontrolled mobilization poses a major threat to genome integrity by disrupting gene expression and inducing DNA damage (Kazazian, 2004; Goodier and Kazazian, 2008; Hedges and Belancio, 2011; Betancourt et al., 2024). In the gonads of *Drosophila melanogaster*, TE activity is repressed by PIWI-interacting RNAs (piRNAs), a class of 23–29 nt small non-coding RNAs that associate with PIWI-clade Argonaute (Ago) family proteins, Piwi, Aubergine (Aub), and Ago3 to form piRNA-induced silencing complexes (piRISCs). These complexes mediate both transcriptional and post-transcriptional silencing of TEs, thereby safeguarding germline genome integrity (Brennecke et al., 2007; Czech and Hannon, 2011; Darricarrère et al., 2013).

piRNAs are derived from long precursor transcripts generated at discrete genomic loci known as piRNA clusters, which serve as reservoirs of TE fragments and subsequently produce antisense piRNAs against active elements (Brennecke et al., 2007; Malone and Hannon, 2009). In *Drosophila*, piRNA clusters are classified into two distinct clusters: dual-strand clusters which are transcribed from both genomic strands, and uni-strand clusters, transcribed from a single strand. The *flamenco* locus functions as the major uni-strand cluster in ovarian somatic cells, whereas *42AB* and *38C* represent the predominant germline dual-strand clusters that contribute to most piRNA production in ovarian germline cells (Brennecke et al., 2007; Goriaux et al., 2014; Andersen et al., 2017). In *Drosophila* germline cells, these dual-strand piRNA precursors are exported from the nucleus to specific membrane-less granules termed nuage in the perinuclear cytoplasmic region, mediated by the Nxf3-Nxt1 export pathway (ElMaghraby et al., 2019; Kneuss et al., 2019; Mendel and Pillai, 2019; Lin et al., 2023). piRNA precursors and transposon transcripts are subsequently loaded onto

Aub and Ago3 by the function of RNA helicases such as Vas to initiate the amplification process known as the ping-pong cycle (Xiol et al., 2014). During this process, Aub and Ago3 engage in reciprocal cleavage of target transcripts with a 10-nt overlap at 5'-ends, producing sense and antisense piRNAs for repressing TEs (Brennecke et al., 2007; Gunawardane et al., 2007; Aravin et al., 2007; Lim et al., 2014).

In addition to Aub and Ago3, a set of nuage-localizing proteins are indispensable for precursor processing and ping-pong amplification of piRNAs. Notably, Tejas (Tej), a Tudor-domain-containing protein, functions as a molecular scaffold that recruits the RNA helicases Vasa (Vas) and Spindle-E (Spn-E) to nuage, thereby facilitating both piRNA precursor processing and the dynamic assembly of functional piRNA complexes (Lim and Kai, 2007; Nishida et al., 2007; Malone et al., 2009; Patil and Kai, 2010; Xiol et al., 2014; Sato et al., 2015; Lin et al., 2023; Adashev et al., 2024). Other nuage components, such as Krimper (Krimp) and Qin/Kumo, also act as regulators of PIWI-family protein interactions and strand-biased production of piRNAs during ping-pong amplification (Zhang et al., 2011; Anand and Kai, 2012; Sato et al., 2015). Taken together, these proteins form a highly coordinated network within the nuage that ensures robust piRNA biogenesis.

By contrast, the molecular functions of certain nuage components remain poorly understood. Squash (Squ), a *Drosophila*-specific protein, was initially proposed as an RNAse HII-related protein (Pane et al., 2007), yet structural prediction by the AlphaFold program suggested that it is an intrinsically disordered protein lacking any conserved or characterized motifs/domains (Kawaguchi et al., 2025). Squ has been implicated to function in piRNA biogenesis in *Drosophila*: upon loss of *squ* function, upregulation of some TEs and a mild reduction of total piRNAs are observed, while no severe disruption for the localization of core piRNA components is detected (Pane et al., 2007; Malone et al., 2009; Kawaguchi et al., 2025). Although *squ* mutant females can produce eggs, a range of dorsoventral (DV) patterning defects are observed in mutant oocytes and the eggs from *squ* mutant mother cannot hatch (Schüpbach and Wieschaus,

1991; Pane et al., 2007). In this study, we identified Squ as a crucial partner of Spn-E, orchestrating the ping-pong amplification of piRNAs and piRNA processing from Aub to Ago3 at nuage. Also, Squ sustains controlled heterotypic ping-pong amplification between Aub and Ago3 by maintaining Ago3 protein level in *Drosophila* germline cells.

Results

Nuage component Squ is specifically required for Ago3 abundance

Previous studies reported that loss of *squ* reduces total piRNAs by ~50% without markedly altering the nuage localization of core ping-pong factors such as Aub and Ago3 (Pane et al., 2007; Malone et al., 2009). Immunostaining of the control ovaries showed that endogenous Squ was enriched in the perinuclear nuage granules of nurse cells (Fig. 1A). This finding was consistent with previous observations using a transgene expressing HA-tagged Squ, confirming the localization of Squ to the nuage (Pane et al., 2007). To further examine the molecular role of Squ, we analyzed the localization and abundance of major piRNA pathway components in *squ* mutant ovaries using the trans-heterozygous alleles, $squ^{PP32/HE47}$(hereafter, *squ* mutant). In *squ* mutant ovaries, the perinuclear signals of most core ping-pong factors (Spn-E, Aub, Vas and Tej) were largely unaffected (Fig. 1A). Reversely, in the mutant of *spn-E*, *vas*, or *tej*, Squ protein level was decreased and detected only faintly in the cytoplasm (Fig. 1B, C and Fig. S1A, B), indicating that Squ is not an indispensable factor for nuage formation but rather a factor recruited by these core ping-pong factors to nuage.

We found, in the immunofluorescence observations of *squ* mutant ovaries, Ago3 signal is markedly weak (Fig. 1A). Consistently, immunoblotting of *squ* mutant ovarian lysate revealed a reduction in Ago3 protein level by ~80% compared to those in wild-type condition, whereas Aub, Spn-E, Vas and Tej were largely unchanged (Fig. 1D and E). Hence, this reduction is Ago3-specific. Ovarian transcriptome analysis confirmed that *ago3* mRNA level was essentially unchanged in *squ* mutant ovaries ($\log_2$FC = -0.19, padj

121 = 0.07; Fig. 1F). Taken together, these data suggest that *squ* is critical in maintaining Ago3
122 protein abundance in germline cells.
123
124 ***squ* loss derepresses germline-specific transposons**
125 Given the severe loss of Ago3 in *squ* mutant ovaries (Fig. 1), TEs might be
126 derepressed. Indeed, RNA-seq analysis revealed that many TEs were significantly up-
127 regulated in *squ* mutant ovaries (24 out of 119 TE families showed $\log_2FC > 1$, p-value <
128 0.05; Fig. 2A). Consistent to the expression of Squ in germline cells (Fig. 1A), these
129 upregulated TEs mostly belonged to germline-specific families (Fig. 2B, S2A; Durdevic
130 et al., 2018; Kneuss et al., 2019). RT-qPCR confirmed significant up-regulation of
131 representative germline TEs, *HMS-Beagle*, *Burdock* and *blood*, in *squ* mutant ovaries (Fig.
132 2C). As an independent protein-level readout of de-repression, we examined a canonical
133 piRNA-controlled target, HeT-A, by immunostaining and detected robust increase of
134 HeT-A Gag protein in oocyte of *squ* mutant ovaries—which is normally silenced by the
135 piRNA pathway (Fig. 2D; Shpiz et al., 2011). Together, these data indicate that *squ* is
136 required to repress a broad set of germline TEs.
137
138 **Squ is required for maintenance of Ago3-bound piRNAs and stalls piRNA precursor**
139 **processing at nuage**
140 The de-repression of TEs always represents the reduction of piRNA production and
141 previous study has already reported that the total number of piRNAs was reduced to half
142 in *squ* mutant ovaries (Malone et al., 2009). However, the cause of the reduction in
143 piRNAs remain unclear. To address this question, we analyzed 23-29 nt small RNAs
144 bound to Aub and Ago3. NGS analysis revealed that the amount of Ago3-bound piRNAs
145 from piRNA clusters *38C-3* and *42AB* were strongly depleted in *squ* mutant ovaries but
146 that of Aub-bound piRNAs were not largely affected (Fig. 3A, rep1; Fig. S3A, rep2).
147 Although without significant reduction for Aub-bound piRNAs, the antisense bias of
148 Aub-bound piRNAs mapping to transposons was reduced from ~77% to ~55% in *squ*

149 mutant ovaries (Fig. 3B and S3B). Of those, Aub-bound piRNAs mapping to severely
150 upregulated TEs in *squ* mutant ovaries, such as *HMS-Beagle*, *blood*, *Burdock* and *HeT-A*,
151 showed severe reduction of antisense bias (Fig. 3C and S3C), implying that this reduction
152 of antisense bias may further result in upregulation of corresponding TEs. Take together,
153 these data suggest that Squ is required for efficient production for Ago3-bound piRNAs,
154 which in turn maintains the antisense enrichment of Aub-bound piRNAs for effective
155 transposon silencing.

156 As precursor processing disruption always results in piRNA reduction, we next
157 examined whether the recruitment of piRNA precursors to perinuclear nuage was
158 perturbed upon loss of *squ* function. Hybridization chain reaction–fluorescence in situ
159 hybridization (HCR–FISH; Choi et al., 2018) targeting precursors from the major dual-
160 strand clusters in germline cells, *38C* and *42AB*, showed accumulated perinuclear signals
161 in *squ* mutant nurse cells compared with controls (Fig. 3D). Quantification using a
162 perinuclear-rim index (Lin et al., 2023) revealed that ~45% of the total precursor signal
163 resided at the perinuclear rim in *squ* mutant nurse cells vs ~20% in heterozygous controls
164 (Fig. 3E). This perinuclear accumulation in *squ* mutant ovaries is comparable to that
165 reported for *vas*, *tej*, and *spn-E* mutants, which function on recruiting precursors or TE
166 transcripts to initiate the ping-pong amplification at nuage (Lin et al., 2023). Consistently,
167 piRNA-cluster transcripts were increased in *squ* mutant ovaries by RT-qPCR (Fig. S3D).
168 Because signals remained predominantly cytoplasmic rather than nuclear, these
169 observations argue against a primary nuclear-export defect and instead suggest inefficient
170 precursor processing in perinuclear nuage upon loss of *squ* function. Taken together, these
171 findings place *squ* as a factor required for Ago3-bound piRNA production and the
172 efficient perinuclear processing of piRNA precursors.

173

174 **Low Ago3 protein level in *squ* mutant triggers Aub-Aub homotypic ping-pong**

175 In *Drosophila* germline cells, the canonical 'ping-pong' amplification loop also
176 known as 'heterotypic ping-pong' occurs between Aub (antisense, 1U bias for bound

177 piRNA) and Ago3 (sense, 10A bias for bound piRNA), but in *kumo*/*qin* and *krimp* mutants,
178 different extents of reduction for Ago3 protein level were detected together with a piRNA
179 production step called 'homotypic ping-pong' occurred by Aub with itself harboring a
180 '1U10A' bias for bound piRNAs (Zhang et al., 2011; Sato et al., 2015). To test whether
181 the low Ago3 level elicits Aub-Aub homotypic ping-pong, we examined piRNA profiles
182 in *squ* and *ago3* mutant ovaries. The 1U nucleotide bias of Aub-bound piRNAs and 10A
183 bias of Ago3-bound piRNAs were detected in controls, as expected (Fig. 4A). In contrast,
184 Aub-bound piRNAs in *squ* mutant ovaries exhibited a strong '1U10A' signature, a
185 hallmark of Aub-Aub homotypic ping-pong (Fig. 4A and S4A), whereas Ago3-bound
186 reads were too few to assess. Importantly, in *ago3* mutant ovaries, we also observed a
187 strong '1U10A' signature for Aub-bound piRNAs (Fig. 4B and S4B), the characteristic
188 for Aub-Aub homotypic ping-ping, together with the reduction for antisense bias in line
189 with the previously reported up-regulation of transposons like *HMS-Beagle*, *blood*,
190 *Burdock* and *HeT-A* (Fig. 4C-E and S4C-E; Li et al., 2009). These data suggest that the
191 role of Squ in maintaining Ago3 protein level is crucial for sustaining the heterotypic
192 ping-pong cycle in *Drosophila* germline cells.
193
194 **Squ–Spn-E interaction is essential for piRNA precursor processing and TE**
195 **repression**
196 In previous studies, Squ protein was detected, together with several piRNA factors,
197 in immunoprecipitates of Spn-E from ovarian lysates, indicating that Squ and Spn-E
198 interact either directly or indirectly (Andress et al., 2016). Recently, AlphaFold2
199 predicted their direct interaction with high confidence, and co-immunoprecipitation
200 assays in S2 culture cells confirmed this specific interaction between Squ and Spn-E
201 (Kawaguchi et al., 2025). Consistently, Squ co-immunoprecipitated with Spn-E from
202 ovarian lysates, reflecting a specific interaction *in vivo* (Fig. 5A). A faint signal with
203 Ago3 was also observed (Fig. 5A and S5A), whereas Aub, Vas, and Tej were

undetectable in the Squ-immunoprecipitants, indicating that Squ preferentially associates with Spn-E, and only a minor potential interaction with Ago3.

To investigate the molecular basis and physiological relevance of the Squ–Spn-E interaction, we first examined the interface predicted by AlphaFold2. Four residues in Squ (E107, E109, R115, and K163), which are conserved in *Drosophila* Squ homologs shown in our previous study (Kawaguchi et al., 2025), are predicted to form salt bridges with four corresponding residues in Spn-E (K834, R675, D640, and E1274). Substituting these four residues with alanine in Squ (Squ^{4A}) abolished its interaction with Spn-E in S2 cells (Kawaguchi et al., 2025). To complement this, in this study, we generated Spn-E mutant with alanine substitutions at the predicted interface residues ($Spn\text{-}E^{4A}$), which likewise lost binding to Squ in co-immunoprecipitation assays in S2 culture cells (Fig. S5B), collectively confirming that these conserved residues mediate the interaction via salt bridges.

To assess the physiological consequences of disrupting this interaction *in vivo*, Squ^{4A} or wild-type Squ (Squ^{WT}) was expressed under the native promoter in ovaries lacking endogenous *squ*. Co-immunoprecipitation revealed markedly reduced binding of Squ^{4A} to Spn-E compared with Squ^{WT} in ovaries (Fig. 5B). Besides, Squ^{4A} showed detached aggregates in the cytoplasm in addition to the perinuclear foci and was expressed at lower levels than Squ^{WT} (Fig. 5C and S5C). Rescue experiments further demonstrated that Squ^{WT} restored proper localization of piRNA precursors, processing of piRNA cluster transcripts as reflected by reduction of their levels (Fig. 5D and S5D), repression of TEs and suppression of HeT-A Gag protein accumulation (Fig. 5E and F). Moreover, Squ^{WT} restored female fertility as measured by hatching rates (Fig. S5E). In contrast, Squ^{4A} failed to rescue any of these defects despite with a higher expression than endogenous Squ (Fig. 5C-F and S5C-E). Collectively, these results indicate that the four conserved residues in Squ are critical for direct binding to Spn-E *in vivo* and this interaction is essential for proper piRNA biogenesis, TEs' repression, and female fertility in *Drosophila*.

232 **Squ contributes to Ago3 protein maintenance independently of Spn-E**

233 In *squ* mutant ovaries, both Ago3 immunostaining signals and total protein levels
234 were severely reduced (Fig. 1). This reduction was efficiently rescued by expression of
235 Squ^{WT}, whereas the Squ^{4A} mutant protein restored Ago3 only weakly (Fig. 6A and B),
236 suggesting that Squ contributes to the maintenance of Ago3 protein levels. To further
237 examine whether the Squ–Spn-E complex is required for the Ago3 stability or Squ has a
238 direct effect on maintaining Ago3 protein, Ago3 localization and protein levels were
239 analyzed by expressing Squ^{WT} or Squ^{4A} in the *spn-E* mutant background. Previous studies
240 have reported a strong reduction of Ago3 protein in *spn-E* mutant ovaries (Ryazansky et
241 al., 2016; Andress et al., 2016), which we also confirmed with our newly generated loss
242 of function allele, $spn\text{-}E^{7\text{-}4}$, in this study. Upon the loss of *spn-E* function, Ago3 protein
243 level was strongly reduced together with a pronounced decrease in endogenous Squ (Fig.
244 6C). Notably, the expression of Squ^{WT} substantially increased Ago3 abundance in *spn-E*
245 mutant ovaries, suggesting that Squ^{WT} stabilizes Ago3 protein in a Spn-E-independent
246 manner. On the other hand, the Squ^{4A} mutant had only a minor effect on the level of Ago3,
247 which may be due to its lower expression level and/or the impaired functional activity of
248 the mutant protein (Fig. 6C).

249 To test whether Squ associates with Ago3 independently of Spn-E, we performed co-
250 immunoprecipitation assays in the *spn-E* mutant background. Both Squ^{WT} and Squ^{4A} were
251 found to associate with Ago3 even in the absence of Spn-E (Fig. S6A), indicating that
252 Squ can interact with Ago3 independently of Spn-E. In contrast, overexpression of Flag-
253 Ago3 by a strong germline driver, NGT40 and nosGal4, in *squ* mutant ovaries failed to
254 restore Ago3 protein levels (Fig. S6B), indicating that Squ is required for Ago3 protein
255 stabilization rather than for Ago3 expression itself. Together, these results suggest that
256 although proper Squ–Spn-E function is required for robust maintenance of Ago3 protein,
257 Squ also exerts a Spn-E–independent effect on Ago3 protein stability through an as-yet-
258 unknown mechanism.

259 To determine whether the defects in piRNA precursor processing and transposon

260 repression in *spn-E* mutant ovaries are primarily caused by Ago3 reduction, we analyzed
261 the expression of piRNA cluster transcripts from *38C* and *42AB*, as well as the
262 retrotransposon *HeT-A* in *spn-E* mutant ovaries (Fig. 6D). Despite the substantial
263 restoration of Ago3 protein levels by Squ^{WT} expression, the upregulation of cluster
264 transcripts and *HeT-A* remained largely unchanged in *spn-E* mutant ovaries (Fig. 6D).
265 Similar results were observed with Squ^{4A} (Fig. 6D). These results indicate that recovery
266 of Ago3 protein alone is not sufficient to rescue the defects in piRNA precursor processing
267 or transposon repression in *spn-E* mutant ovaries. Instead, it implies that Spn-E acts
268 upstream of both Squ and Ago3 in the piRNA pathway, supporting the notion that Spn-E
269 is a core nuage factor essential for piRNA pathway activity.
270
271 **Squ facilitates Spn-E–mediated RNA processing at Aub**
272 A recent study in silkworm demonstrated that Spn-E is recruited to the Siwi (the
273 silkworm ortholog of *Drosophila* Aub)–piRNA–target RNA complex formed with
274 GTSF1 and Meal (referred to as Siwi* or Aub*) (De et al., 2025). To examine whether
275 the formation or dynamics of the Aub*–Spn-E complex is affected by Squ, we analyzed
276 the interaction between Aub and Spn-E by immunoprecipitation. When Aub was
277 immunoprecipitated from control ovary lysates, Spn-E was barely detectable in the bound
278 fraction. In contrast, the amount of Spn-E co-precipitated with Aub was increased in *squ*
279 mutant ovaries (Fig. 7A and S7A). These results indicate that Spn-E remains more stably
280 associated with Aub* in the absence of Squ. To further examine the nature of this Aub*–
281 Spn-E complex, we analyzed the RNA species recovered in the Spn-E
282 immunoprecipitants. The levels of piRNA cluster transcripts derived from *38C* and *42AB*,
283 which serve as major target RNAs for Aub, were significantly increased in *squ* mutant
284 ovaries compared with the heterozygous controls, despite a similar amount of Spn-E
285 being present in the IP fractions (Fig. 7B and S7B). These data indicate that, in the absence
286 of Squ, Spn-E is retained on the Aub* complex together with piRNA precursor transcripts,
287 which are not efficiently processed further. As the interaction between Squ and Spn-E has

been predicted by AlphaFold program and verified by the mutational analysis (Kawaguchi et al., 2025), and importantly, the predicted Squ-binding interface on Spn-E is located on the surface opposite to the Aub*-binding interface (Fig. S7C), suggesting that Squ does not directly compete with the Spn-E–Aub* interaction.

As an RNA helicase protein, Spn-E is expected to possess RNA-binding and ATPase activities (Ott et al., 2014), so we next examined whether Squ directly affects the ATPase activity of Spn-E. Purified wild-type Spn-E protein (Spn-E^{WT}) exhibited basal ATP hydrolysis activity *in vitro*, whereas the ATPase-dead mutant, Spn-E^{DQVH}, showed no detectable ATPase activity (Fig. S7D). Squ protein alone also did not exhibit ATPase activity (Fig. S7D). Notably, the addition of Squ did not significantly alter the ATP hydrolysis activity of Spn-E^{WT} in these *in vitro* conditions (Fig. S7D). Together, these results demonstrate that, although Squ does not disrupt Aub*–Spn-E binding directly and affect the basal ATPase activity of Spn-E *in vitro*, loss of Squ leads to persistent retention of Spn-E on the Aub* complex together with piRNA precursor transcripts *in vivo*. This aberrant accumulation of the Aub*–Spn-E–RNA intermediate provides a mechanistic explanation for why piRNA precursor processing and downstream piRNA pathway function remain defective in conditions where Ago3 protein levels can be partially restored by Squ in the *spn-E* mutant background.

Discussion

The piRNA pathway, which represses transposable elements, is well conserved across virtually all animals examined to date, including *Drosophila melanogaster*. In *Drosophila* germline cells, piRNA amplification occurs in the membrane-less perinuclear organelle known as nuage, where multiple piRNA pathway components localize (Aravin et al., 2006; Hirano et al., 2014; Lim and Kai, 2015; Suyama and Kai, 2024). However, the precise mechanisms underlying piRNA biogenesis and the molecular functions of individual nuage components remain elusive. In this study, we

315 systematically characterized the molecular role of Squ, a *Drosophila*-specific nuage
316 protein, and uncovered its dual functions in piRNA pathway: facilitating Spn-E–
317 dependent RNA processing and maintaining Ago3 protein stability (Fig. 7C).
318 Our results suggest that Squ functions as a co-factor of Spn-E, an RNA helicase and
319 facilitates the efficient transfer of sliced RNA intermediates from Aub to Ago3 during
320 the ping-pong amplification cycle. RNA helicases generally utilize their ATPase activity
321 to unwind RNA structures or release a single-stranded RNA from the duplexes
322 (Jankowsky and Fairman, 2007; Jankowsky, 2011). Considering this general property,
323 Spn-E–dependent RNA remodeling is likely required for efficient heterotypic ping-pong
324 between Aub and Ago3. In support of this concept, the ATPase activity of another
325 nuage-localized RNA helicase, Vas, is stimulated by the nuage factor Tejas (Tej) through
326 its Lotus domain in the presence of single-stranded RNA (Xiol et al., 2014; Jeske et al.,
327 2017). Notably, Tej, like Squ, also binds Spn-E (Lin et al., 2023), suggesting that
328 multiple nuage factors may cooperate to regulate Spn-E activity. In this study, we
329 detected the intrinsic ATPase activity of Spn-E *in vitro*; however, Squ did not
330 significantly enhance Spn-E ATPase activity (Fig. S7D). We speculate that Tej and/or
331 other yet-unidentified Spn-E interacting proteins may serve as primary activators of
332 Spn-E *in vivo*, and these may associate with the Aub*–Spn-E–Squ complex (Fig. S7C).
333 Further experiments are still necessary to elucidate the enzymatic activity of Spn-E and
334 its functional relevance *in vivo*.
335 Previously, we reported that Squ and Spn-E expressed in S2 cells, a somatic cell
336 line that lacks germline-specific piRNA factors, can directly bind each other. Four
337 interacting residue-pairs between Squ and Spn-E are conserved in *Drosophila* species
338 and mutation of four conserved interacting residues in Squ (Squ^{4A}) abolishes this
339 interaction in S2 cells (Kawaguchi et al., 2025). In this study, we further confirmed that
340 Squ^{4A} also fails to properly interact with Spn-E *in vivo* using transgenic expression in
341 the ovary, and that reciprocal mutation of the corresponding residues in Spn-E (Spn-
342 E^{4A}) similarly abolishes its interaction with Squ in S2 culture cells (Fig. 5B; Fig. S5B).

343 Importantly, Squ^{4A} failed to rescue the piRNA-deficient phenotypes of the *squ* mutant
344 ovaries (Fig. 5 and S5). Nevertheless, a substantial fraction of Squ^{4A} remained
345 detectable in the perinuclear nuage region (Fig. 5C). A similar discrepancy between
346 physical interaction and nuage localization has been reported for Tej: although Tej-$^{\Delta}$SRS
347 loses its ability to interact with Spn-E in S2 culture cells, it does not disrupt the nuage
348 localization of Spn-E or Vas *in vivo*, whereas a bit larger, extended SRS deletion is
349 required to abolish their interaction (Lin et al., 2023). These observations suggest that
350 the highly condensed molecular environment of nuage and/or additional protein
351 interactions can maintain nuage localization even when direct interactions with Spn-E
352 are weakened or disrupted.
353 Consistent with the reduced Ago3 protein level in *squ* mutant, heterotypic ping-
354 pong between Aub and Ago3 was severely compromised (Fig. 4), whereas Aub protein
355 level was not affected (Fig. 1C). Because Aub–Aub homotypic ping-pong activity was
356 clearly detected in *squ* mutant ovaries, we propose that, when Ago3 is non-functional,
357 sliced RNAs are transferred from one Aub molecule to another to sustain this alternative
358 cycle (Fig. 7C). This homotypic pathway, although active, is less efficient in piRNA
359 production and transposon repression than the heterotypic pathway. Aub–Aub
360 homotypic ping-pong has also been reported in *krimp* and *qin*, also known as *kumo*,
361 mutant ovaries; Krimp promotes Aub–Ago3 coupling through its Tudor-domain–
362 mediated dimerization, and Qin/Kumo is likewise required for Aub–Ago3 association
363 (Zhang et al., 2011; Anand and Kai, 2012; Sato et al., 2015). These observations suggest
364 that efficient heterotypic ping-pong is supported by the coordinated actions of multiple
365 regulatory factors, whereas the Aub–Aub cycle can become prominent when this
366 regulatory network is perturbed. In this study, we show that Squ as one such regulatory
367 factor that promotes heterotypic ping-pong through its functional coupling with Spn-E
368 (Fig. 7C).
369 Our results demonstrate that Squ is essential for maintaining Ago3 protein stability.
370 Loss of Squ led to a marked reduction of Ago3 protein level and Ago3-bound piRNAs,

while *ago3* transcript level was not affected (Fig. 1E-F, 3A). These results suggest that Squ regulates Ago3 via a post-transcriptional mechanism. It has been reported that unloaded Piwi protein is destabilized and degraded (Sienski et al., 2012; Kina et al., 2025), and we therefore propose that the piRNA-free, ‘‘empty’’ form of Ago3 may likewise be subjected to proteasome-dependent turnover. However, ectopic expression of Squ in *spn-E* mutant ovaries restored Ago3 protein abundance despite the severe reduction in piRNA production caused by loss of *spn-E* function, implying that Squ may possess an additional, direct role on stabilizing Ago3 protein (Fig. 6). Notably, restoration of Ago3 protein level in *spn-E* mutant did not rescue piRNA precursor processing defects and transposon de-repression, indicating that *spn-E* is genetically epistatic to *squ* and *ago3* function. These results uncover a functional hierarchy among nuage components, where Squ contributes to transposon repression by supporting both Spn-E–mediated precursor processing and Ago3 stability via an unresolved post-transcriptional mechanism.

Taking together, our results refine the current model of piRNA biogenesis in *Drosophila* germline cells. Squ functions on stabilizing Ago3 protein for heterotypic ping-pong between Aub and Ago3. Squ also acts as a crucial co-factor of Spn-E in the nuage, promoting piRNA precursor turnover or facilitating transfer of sliced transcripts between ping-pong partners. Further studies are needed to elucidate the molecular mechanism for Squ to perform these functions. Understanding these mechanisms will provide deeper insights into the piRNA production mechanism cooperated by many regulatory proteins.

Materials and Methods

Fly stocks

All fly stocks were maintained at 25°C on standard food (5% (w/v) dry yeast, 5% (w/v) corn flower, 2% (w/v) rice bran, 10% (w/v) glucose, 0.7% (w/v) agar, 0.2% (v/v) propionic acid, and 0.05% (w/v) p-hydroxy butyl benzoic acid). The mutant alleles used

399 in this study were *squ*$^{PP32/HE47}$ (Pane et al., 2007), *ago3*$^{g1/g2}$ (VDRC #313531; VDRC
400 #313532; Senti et al., 2015), *spn-E*$^{7-4}$ (this study), *tej*$^{48-5}$/Df(2R) Exel7131 (Patil and
401 Kai, 2010; BL #7876), *vas*$^{4-2}$ (this study) and *krimp*^{f06583}/Df(2R) Exel6063 (BL #18990,
402 Lim and Kai, 2007; BL #7545). The heterozygotes of individual mutants were used as
403 the control conditions. Knock-In fly line *aub*$^{EGFP.KI}$ (DGRC #118621, Kina et al., 2019)
404 and transgenic fly line UASp-3xFlag.AGO3.WT (DGRC #118699) were obtained from
405 the *Drosophila* Genetic Resource Center at the Kyoto Institute of Technology, Japan.
406 *tej*$^{EGFP.KI}$ was generated in our laboratory (Lin et al., 2023). NGT40-Gal4; *nos*-Gal4-
407 VP16 (Grieder et al., 2000) was used as germline driver line. The genotypes of all fly
408 strains are listed in Table S1.
409
410 **Generation of knock-out flies**
411 Loss of function alleles, *spn-E*$^{7-4}$ and *vas*$^{4-2}$, were generated using the CRISPR/Cas9
412 system. Guide RNAs (gRNAs) targeting the *spn-E* and *vas* loci were designed and
413 cloned into pDCC6 vector, respectively (Gokcezade et al., 2014). The sequences of the
414 gRNAs were: Spn-E gRNA: 5' -GTGCCCAACCGCGAGTTGAT-3' and Vasa gRNA:
415 5'-GGGGATACAATCACTACCTG-3'. Obtained gRNA expression plasmids (120
416 ng/μl) were injected into *y w* embryos. PCR-amplified genomic fragments from
417 candidate lines were subjected to Sanger sequencing, which revealed that *spn-E*$^{7-4}$
418 contains an 8-bp deletion, GCGAGTTG, at 15837616-15837623 (release=r6.53),
419 together with a 4-bp insertion, AACA, causing a frameshift and premature stop codon.
420 Similarly, *vas*$^{4-2}$ carries a 4-bp deletion, GTAG, at 15072945-15072948 (release=r6.53),
421 causing a frameshift leading to premature termination. Loss of the corresponding
422 protein products was confirmed by western blotting and immunostaining using anti-
423 Spn-E and anti-Vas antibodies, respectively.
424
425
426

427 **Generation of transgenic flies**

428 The transgenic fly lines carrying native squ promoter-GFP-3xFlag-Squ^{WT} (pNative-
429 Squ^{WT}) or -Squ^{4A} (pNative-Squ^{4A}) were generated using PhiC31-mediated integration
430 system. The DNA fragments encoding Squ^{WT} or Squ^{4A} were amplified from pENTR-
431 Squ^{WT} and Squ^{4A} plasmids, respectively (Kawaguchi et al., 2025). The fragments of
432 promoter region, 5'UTR and 3'UTR were amplified by PCR from genomic DNA. GFP-
433 3xFlag fragment was amplified from the plasmid containing GFP-3xFlag-tag sequence.
434 All the fragments are combined and cloned into pUASt-attB vector (Brand and
435 Perrimon, 1993) by the reaction of In-Fusion® Snap Assembly Master Mix (Takara).
436 The generated constructs were introduced into attP2 site (BDSC#25710).

437

438 **Antibodies**

439 Polyclonal rabbit anti-mKate2 antibody was generated in this study. His-tagged full-
440 length mKate2 was expressed in *Escherichia coli* BL21(DE3) from the pDEST17
441 (Thermo Fisher Scientific) plasmid carrying the mkate2 coding sequence. His-tagged
442 mkate2 protein was solubilized with 6 M urea in PBS and purified using Nickel
443 Sepharose beads (GE Healthcare) according to the manufacturer's protocol. The
444 antibodies used in this study were rat anti-Squ (1:1000, Kawaguchi et al., 2025), guinea
445 pig anti-Aub (1:1000, Lim et al., 2022), mouse monoclonal anti-Ago3 (1:500, National
446 Institute of Genetics, Japan), guinea pig anti-Vas (1:2000, Patil and Kai, 2010), rat anti-
447 Spn-E (1:500, Patil and Kai, 2010), rat anti-Tej (1:500, Lin et al., 2023), guinea pig anti-
448 Krimp (1:1000, Lim and Kai, 2007), guinea pig anti-Ago2 (1:100, Lin et al., 2023),
449 rabbit anti-mkate2 (1:1000, this study), rabbit anti-HeT-A Gag polyclonal antibody
450 (1:1000, Lin et al., 2023), mouse monoclonal anti-Tubulin (1:1000, DM1A, sc-32293,
451 Santa Cruz Biotechnology). The secondary antibodies used in this study were HRP-
452 conjugated goat anti-guinea pig (1:1000, Dako, Cat. #P0141), HRP-conjugated goat
453 anti-rat (1:1000, Dako, Cat. # P0450), HRP-conjugated goat anti-mouse (1:3000,
454 BioRad, Cat. # 1706516) and HRP-conjugated goat anti-rabbit (1:3000, BioRad, Cat.

455 #1706515). ANTI-FLAG® M2-Peroxidase (1:1000, Sigma, Cat. #A8592) and HRP-
456 conjugated anti-Myc-tag antibody (1:1000, MBL, Cat. # M192-7) were also used.
457
458 **Western blotting**
459 Ovaries were homogenized in the ice-cold PBS and denatured in the presence of 1×SDS
460 sample buffer at 95°C for 5 min. The protein samples were subjected to SDS-PAGE and
461 transferred to ClearTrans SP PVDF membrane (Wako). Primary and secondary antibodies
462 described above were diluted in the Signal Enhancer reagent HIKARI (Nacalai Tesque).
463 Chemiluminescence was induced by the Chemi-Lumi One reagent kit (Nacalai Tesque)
464 and detected by ChemiDoc Touch (Bio-Rad). The immunoblotting signals were
465 quantified using ImageJ (Schneider et al., 2012) or Image Lab software (Bio-Rad).
466
467 **RNA immunoprecipitation**
468 To analyze RNAs interacting with proteins, we followed the methods described
469 previously (Lin et al., 2023). To extract Aub- and Ago3-bound piRNAs, and Spn-E–bound
470 RNAs, 300 ovaries (Aub), 500 ovaries (Ago3) and 400 ovaries (mKate2-Spn-E) were
471 dissected from 1-day-adult females in cold PBS buffer. Ovaries were homogenized in
472 lysis buffer containing 20 mM Tris-HCl (pH 7.4), 200 mM NaCl, 2 mM DTT, 10% (v/v)
473 glycerol, 2 mM $MgCl_2$, 1% (v/v) Triton X-100, 1× cOmplete protease inhibitor cocktail
474 (Roche), and 1% (v/v) RNaseOUT recombinant ribonuclease inhibitor (Invitrogen). The
475 lysates were cleared by centrifugation at 20,000 ×*g* for 10 min at 4°C three times to
476 remove cell debris. Dynabeads Protein G/A (Invitrogen) pre-equilibrated with lysis buffer
477 were added to the cleared lysates and rotated at 4°C for 1 h for pre-clearing. After
478 clearance, guinea pig anti-Aub (1:10, Lim et al., 2022) or mouse monoclonal anti-Ago3
479 (1:500, NIG) or rabbit anti-mKate2 (1:500, this study) was added to the lysates and
480 incubated for 3 h with gentle rotation at 4°C. Dynabeads Protein G/A were then added to
481 the mixture and incubated at 4°C for 1 h with rotation. After incubation, magnet beads
482 were collected and washed 5 times by wash buffer containing 20 mM Tris-HCl (pH7.4),

400 mM NaCl, 2 mM DTT, 10% (v/v) glycerol, 2 mM $MgCl_2$, 1% (v/v) Triton X-100, 1× cOmplete protease inhibitor cocktail (Roche), and 1% (v/v) RNaseOUT recombinant ribonuclease inhibitor (Invitrogen). After washing, beads were resuspended in 100 µl wash buffer. Ten µl was used for western blotting to check the efficiency of protein immunoprecipitation and the remaining 90 µl solution was used for RNA extraction using TRIzol LS (Invitrogen) following standard manufacturer's protocol. Extracted RNA were stored at -80°C until analysis. For mKate2-Spn-E RNA IP, negative control was performed by adding equal amount of Dynabeads Protein G/A with IP groups but without antibody.

Small RNA sequencing and analysis

To compare Aub- and Ago3-bound piRNAs in two conditions, the amount of Aub or Ago3 proteins in IP samples were equalized using the signals in the immunoblotting analysis. Libraries from Aub- and Ago3-bound RNAs were prepared and sequenced on an Illumina HiSeq 2500 platform (Genome Information Research Center, Research Institute for Microbial Diseases, Osaka University). After adaptor trimming (5'-AGATCGGAAGAGCACACGTCT-3'), reads mapping to miRNA, rRNA, snRNA, snoRNA and tRNA sequences were removed. Remaining reads were size-selected with 23-29 nt and mapped to major piRNA clusters or the consensus sequences of transposable elements using Bowtie allowing up to 3 mismatches (Langmead et al., 2009). piRNA cluster definition was according to previous paper (Brennecke et al., 2007) and TE sequences were from Flybase (Release 6.32). Read counts were normalized with the counts for 21nt-spike RNA (ACATGGCATGGATGAACTATA) which were added equally to individual RNA samples prepared for library construction (Lutzmayer et al., 2017). piRNA cluster-mapping reads were visualized by pyGenomeTracks (Ramírez et al., 2018). Nucleotide preference was visualized by sequence logo using Ggplot2 R ggseqlogo (Wagih, 2017).

511 **Crosslinking immunoprecipitation (CL-IP)**

512 200 ovaries were dissected from 1-day-adult *y w* females in ice-cold PBS and fixed in
513 PBS containing 0.1% (w/v) paraformaldehyde for 20 min on ice. Crosslinking was
514 quenched in 125 mM glycine for 20 min at room temperature. Ovaries were homogenized
515 in CL-IP lysis buffer containing 50 mM Tris-HCl (pH 8.5), 150 mM KCl, 5 mM EDTA,
516 1% (v/v) Triton X-100, 0.1% (w/v) SDS, 0.5 mM DTT, and 1× cOmplete protease
517 inhibitor cocktail. The lysate was incubated at 4°C for 20 min with rotation and then
518 sonicated with Bioruptor (Lin et al., 2023). After centrifugation at 20,000 ×*g* for 10 min
519 at 4°C, the supernatant was collected and diluted with an equal volume of CL-IP wash
520 buffer containing 25 mM Tris-HCl (pH 7.5), 150 mM KCl, 5 mM EDTA, 0.5% (v/v)
521 Triton X-100, 0.5 mM DTT, and 1× cOmplete protease inhibitor cocktail. Pre-washed
522 Dynabeads Protein G/A mixture (1:1) were added for pre-clearance at 4°C for 1 h with
523 rotation. Anti-Squ antibody was added to pre-cleared supernatant with 1:500 dilution and
524 incubated at 4°C overnight. The pre-equilibrated Dynabeads Protein G/A mixture (1:1)
525 were added for binding and incubated at 4°C for 3 h with rotation. After washing three
526 times with CL-IP wash buffer, beads were collected and resuspended in 50 μl of CL-IP
527 wash buffer containing 1× SDS sample buffer. The beads were then boiled at 95°C for 5
528 min and subjected to SDS-PAGE for western blotting analysis. Negative control was
529 performed as the description above.

530

531 **Immunostaining of ovaries**

532 Ovaries were dissected, fixed with 5% (w/v) paraformaldehyde containing PBS for 20
533 min and permeabilized in PBX (PBS with 0.2% [v/v] Triton X-100). The primary
534 antibodies used in this study were described above. Secondary antibodies were Alexa
535 Fluor 488-, 555-, and 633-conjugated goat antibodies at a 1:200 dilution (Thermo Fisher
536 Scientific, United States) and CF®633 goat antibodies at a 1:1000 dilution (Biotium,
537 Fremont, CA, United States). Ovaries expressing endogenous fluorescent-tagged proteins
538 were fixed with 0.1% (w/v) paraformaldehyde containing PBS for 20 min and washed

539 with PBX for 15 min, twice. DAPI was diluted for 1:1000 to stain DNA. Ovaries were
540 equilibrated in Fluoro-KEEPER Antifade Reagent (Nacalai Tesque) and stored at 4°C
541 before mounting. Images were taken by ZEISS LSM 900 with Airy Scan 2 using 63x oil
542 NA 1.4 objectives and processed by ZEISS ZEN 3.0 and ImageJ (Schneider et al., 2012).
543

544 **RNA in situ hybridization chain reaction (HCR)**

545 Probes (Molecular Instruments, *42AB*-LOT: PRJ124; *38C*-LOT: PRJ125) targeting
546 piRNA cluster transcripts from specific regions of cluster *42AB* (Chr2R: 6322410-
547 6323756) and *38C* (Chr2L: 20104896-20213637) were generated and used in this
548 experiment. Commercial reagents were used for this reaction (Molecular Instruments,
549 Inc.) according to the manufacturer's instructions and previously described protocols (Lin
550 et al., 2023).
551

552 **Quantification of in situ-HCR signal for piRNA precursors**

553 Fluorescence intensities for piRNA clusters *38C* and *42AB* were quantified using ImageJ
554 (Fiji) after background subtraction. WGA was used to stain the nuclear envelope, and a
555 region extending ±5% of the nuclear diameter inside and outside the envelope was defined
556 as the perinuclear region, as previously described (Lin et al., 2023).
557

558 **RT-qPCR**

559 Flies were fattened up with moist yeast paste for 2 days and then dissected for RNA
560 extraction using TRIzol LS (Invitrogen) following manufacturer's protocol with DNase I
561 (Invitrogen) treatment. Reverse-transcription was performed by Super Script III system
562 (Invitrogen) using primers of a mixture for d(T)20 and randomized
563 hexadeoxyribonucleotide. KAPA SYBR Fast qPCR Master Mix (KAPA biosystems) was
564 used for qPCR reactions and primer sequences used in this study were listed in Table S2.
565 The relative expression levels were calculated by $^{\Delta\Delta}$Ct method using *rp49* as reference.

566 All the experiments were performed by 3 biological replicates.

567

568 **mRNA-seq**

569 Total RNAs were extracted from *squ* heterozygous and mutant ovaries using TRIzol LS
570 (Invitrogen) following the manufacturer's instruction. Poly(A)+ RNA was enriched using
571 oligo(dT) beads with the NEBNext Poly(A) mRNA Magnetic Isolation Module (New
572 England Biolabs, USA). The enriched RNA was fragmented, reverse-transcribed,
573 adapter-ligated, and PCR-amplified to prepare cDNA libraries using the NEBNext Ultra
574 II Directional RNA Library Prep Kit (New England Biolabs, USA). Library preparation
575 and sequencing were outsourced to Rhelixa (Japan), yielding approximately 35 million
576 reads per sample. Low quality sequences and adapters were removed by fastp (Chen et
577 al., 2018). Paired end reads were mapped to *Drosophila melanogaster* reference genome
578 r6.32 and the canonical sequences of TEs by STAR version 2.7 with default setting.
579 (Dobin et al., 2013). Reads mapped to exons of individual genes and the canonical TEs
580 were counted using featureCounts (Liao et al., 2014). Differential expression analysis was
581 performed by DESeq2 (Love et al., 2014) with significant up-regulation ($Log_2FC>1$, p-
582 adj<0.05) and down-regulation ($Log_2FC<-1$, p-adj<0.05). Two biological replicates were
583 performed for the mRNA-seq analysis.

584

585 **Co-immunoprecipitation in S2 cells**

586 The *Drosophila* S2 cell line (S2-DRSC) was cultured at 28°C in Schneider's medium
587 supplemented with 10% (v/v) fetal bovine serum and antibiotics (penicillin and
588 streptomycin). Protein-coding sequences of *squ* and *spn-E* were amplified and cloned into
589 the pENTR vector (Thermo Fisher Scientific) and subsequently transferred into pAFW
590 or pAMW destination vectors for plasmid construction. S2 cells ($0.2–2 \times 10^6$ cells/ml)
591 were pre-cultured in 12-well plates overnight before transfection with Hilymax (Dojindo
592 Molecular Technologies, Japan). After 36–48 h of transfection, S2 cells were collected
593 for co-immunoprecipitation (co-IP) experiments as previously described (Kawaguchi et

594 al., 2025).

595

596 ***Drosophila* fertility test**

597 Female fertility was assessed by pairing three *y w* males with five females of each
598 genotype in an enclosed environment on apple juice plates supplemented with a small
599 amount of moist yeast paste. The number of eggs laid was recorded after 24 h of mating,
600 and the hatching rate was calculated 24 h after egg laying. Egg counts and hatching
601 rates were recorded for at least 3 consecutive days.

602

603 **Purification of recombinant proteins in Sf9 cells**

604 *Spodoptera frugiperda* Sf9 cells were cultured using ExpiSf^{TM} CD Medium (Thermo
605 Fisher Scientific/Gibco) in 27°C on an orbital shaker platform at 120 rpm. The fragment
606 of DNA product for 6His-2StrepII-GFP-Spn-E^{WT}, -Spn-E^{DQVH} or -Squ^{WT} was amplified
607 and inserted into pFastBac1 vector (Thermo Fisher Scientific). Recombinant
608 baculoviruses expressing 6His-2StrepII-GFP–Spn-E^{WT}, –Spn-E^{DQVH}, or –Squ^{WT} were
609 generated using the NucleoBond® Xtra BAC kit (Clontech/Takara) and used to infect
610 Sf9 cells according to the manufacturer's protocol (Thermo Fisher Scientific). After
611 several days, infected Sf9 cells were resuspended in 10 ml lysis buffer: 100 mM Tris-
612 HCl (pH 8.0), 150 mM NaCl, 1% TritonX-100, 1 mM DTT, 1x cOmplete protease
613 inhibitor cocktail (PIC, Roche) and 1 mM PMSF, sonicated for total 10 min with 1 min
614 on/1 min off on the ice and centrifuged for 1 h at 15,000 ×g to collect the supernatant. 1
615 ml Strep-Tactin® Sepharose® resin beads (IBA Lifesciences) were added to the Poly-
616 Prep Chromatography Column (Bio-rad) and followed with 10 ml wash buffer: 100 mM
617 Tris-HCl (pH 8.0), 500 mM NaCl, 1 mM DTT and 1 mM PMSF. All supernatant was
618 then loaded into columns and washed with 10 ml wash buffer, protein was eluted by 10
619 ml elution buffer: 100 mM Tris-HCl (pH 8.0), 150 mM NaCl, 1 mM DTT, 5 mM
620 desthiobiotin and 1x PIC. Recombinant proteins were concentrated by vivaspin turbo 15
621 (Nippon Genetics Co., Ltd) and stored in -80°C after rapid freezing by liquid nitrogen.

622 SDS-PAGE and CBB staining were performed to check the purification and quantity for
623 protein.
624
625 **ATPase assay**
626 ATP hydrolysis reactions were performed at 25°C for 1, 2, 3, or 5 h with 25 μM
627 recombinant protein (6His-2StrepII-GFP-Spn-E^{WT}, Spn-E^{DQVH}, or Squ^{WT}) in ATPase
628 assay buffer (10 mM Tris-HCl, pH 8.0, 100 mM NaCl, 2 mM $MgCl_2$, 1 mM DTT, and
629 200 μM ATP (Sigma)). To examine the effect of Squ on Spn-E ATPase activity, Squ
630 protein was added at 25 μM to the Spn-E ATPase reaction mixtures. Inorganic
631 phosphate was quantified using BIOMOL® Green Reagent (Enzo Life Sciences) in 96-
632 well plates according to the manufacturer's protocol. Absorbance at 620 nm was
633 measured with an SH 9000 microplate reader (Corona Electric), background values
634 were subtracted, and phosphate concentrations were normalized to calculate ATP
635 hydrolysis (%) using a phosphate standard curve.
636
637 **Acknowledgments**
638 We are grateful to Wakana Isshiki (The University of Osaka) for generation of Squ
639 antibody, to Haitian Qin (The University of Osaka) for assisting of generation of
640 mKate2 antibody, to Dr. Hilo Yen (The University of Osaka) for generation of *spn-E*
641 and *vas* mutant alleles, to Dr. Ritsuko Suyama (The University of Osaka) for HCR-
642 FISH experiments and data analysis. We are also grateful to Dr Trudi Schüpbach
643 (Princeton University) for generous gifts of *squ* mutant flies. We acknowledge
644 Bloomington *Drosophila* Stock Centre and Kyoto Stock Center for the fly stocks. We
645 also thank for the FBS Core Facility in The University of Osaka for providing access to
646 the LSM 900 and ChemiDoc Touch. We thank for the Center for Medical Research and
647 Education, Graduate School of Medicine, The University of Osaka for microplate reader
648 SH-9000Lab (Corona Electric, Japan). We appreciate the insightful discussion and
649 suggestions from all the members of TK's laboratory.

Author contribution

Conceptualization: X. Xu, S. Kawaguchi, and T. Kai.

Data Curation: X. Xu and S. Kawaguchi.

Formal Analysis: X. Xu and S. Kawaguchi.

Funding Acquisition: S. Kawaguchi and T. Kai.

Investigation: X. Xu.

Methodology: X. Xu, S. Kawaguchi, T. Iki, and T. Kai.

Project Administration: T. Kai.

Resources: S. Kawaguchi, T. Iki and T. Kai.

Software: X. Xu, T. Iki and S. Kawaguchi.

Supervision: S. Kawaguchi, T. Iki and T. Kai.

Validation: X. Xu and S. Kawaguchi.

Writing, Original Draft: X. Xu and S. Kawaguchi.

Writing, Review and Editing: X. Xu, S. Kawaguchi, T. Iki and T. Kai.

Data Availability

NGS data set have been deposited to the DNA Data Bank of Japan (DDBJ) and under BioProject ID PRJDB37636.

Funding

This work was supported by Grant-in-Aid for Transformative Research Areas (A) [21H05275 to T.K.], Grants-in-Aid for Scientific Research [T25K022050 for T.K.], and The University of Osaka D3 Center “Transdisciplinary Research Project” [Na22990007 to S.K.]. X.X. is supported by JST SPRING [J219713005].

678 ## Figure legends

679 **Figure 1. Squ is required for Ago3 abundance and exhibits *spn-E*–dependent nuage**
680 **enrichment**

681 (A) Localization of indicated proteins in stage 4-5 egg chambers of *squ* heterozygous or
682 transheterozygous mutants. Immunostaining; Squ, Spn-E, Vas, Ago3. Fluorescence;
683 eGFP-Aub and Tej-eGFP. Scale bar is 5 μm.
684 (B) Protein level of Squ in control and *spn-E* mutant egg chambers.
685 (C) Immunostaining of Squ in control and *spn-E* mutant egg chambers. Scale bar is 5 μm.
686 (D) Immunoblotting of indicated proteins extracted from ovaries of *squ* heterozygous or
687 mutants.
688 (E) Quantification of Ago3 protein signal intensities. Error bars indicate standard
689 deviation (3 biological replicates). Statistics: unpaired t-test, ****$p < 0.0001$.
690 (F) Ago3 transcript levels in control and *squ* mutant ovaries. Fold change given by
691 differential expression analysis (DESeq2) is shown with adjusted p-value.
692

693 **Figure 2: Loss of *squ* derepresses transposons**

694 (A) Volcano plot shows fold changes of transposon transcript levels in ovaries (*squ* mutant
695 compared to *squ* heterozygous condition). Red circles; significantly upregulated
696 transposons ($\log_2FC > 1$, $p < 0.05$), greed circles; significantly downregulated
697 transposons ($\log_2FC < -1$, $p < 0.05$).
698 (B) Fold changes of TEs' expression upon *squ* loss. Transposons are categorized into
699 germline, somatic, and common groups.
700 (C) RT-qPCR analysis of germline-specific transposons (*blood*, *HMS-Beagle*, *Burdock*).
701 Relative transcript levels are calculated by $^{\Delta\Delta}$Ct using rp49 as reference. Values represent
702 fold changes in *squ* mutant relative to heterozygous controls. Error bars indicate standard
703 deviation (3 biological replicates). Statistical analysis is performed using Student's t-test.
704 **$p < 0.01$.

705 (D) Immunostaining of HeT-A Gag and Squ proteins in control and *squ* mutant ovaries.
706 A yellow arrow indicates HeT-A Gag signals accumulating in oocyte. Scale bar: 5 μm.
707
708 **Figure 3: Squ is required for maintenance of Ago3-bound piRNAs and processing of**
709 **piRNA precursors**
710 (A) Aub- (upper panels) and Ago3-bound (lower panels) small RNAs from control and
711 *squ* mutant ovaries mapped to the major piRNA clusters *38C-3* and *42AB* (replicate 1).
712 Plus-strand (blue) and minus-strand (red) piRNAs are shown as upward and downward
713 peaks, respectively.
714 (B) Antisense bias of Aub-bound piRNAs mapping to transposable elements (TEs) in
715 control (*squ* het) and *squ* mutant ovaries (replicate 1). Each dot represents one TE;
716 antisense piRNA ratios are calculated by dividing antisense-mapping piRNA reads by
717 total mapping reads for each TE. Horizontal lines indicate the mean values. ****$p <$
718 0.0001 (unpaired t-test).
719 (C) Effect of loss of *squ* function on antisense ratio of Aub-bound piRNAs mapping to
720 transposon consensus sequences. Dots indicate 24 up-regulated TEs (Fig. 2A)
721 in *squ* mutant relative to control ovaries (replicate 1). For each TE, the antisense bias
722 in *squ* mutant is divided by that in *squ* heterozygous.
723 (D) HCR-FISH detection of piRNA precursor transcripts from clusters *38C* and *42AB* in
724 control and *squ* mutant ovaries. One representative nucleus for each sample is shown. A
725 white arrow indicates precursor signals accumulating to perinuclear regions. Blue; DNA
726 (DAPI), green; nuclear membrane (WGA). Scale bar: 2 μm.
727 (F) Quantification of piRNA precursor signals accumulating in perinuclear regions.
728 Fluorescence intensity of precursor foci within ±5% of nuclear diameter from the nuclear
729 membrane is measured (n=10 nuclei per genotype). Signals are plotted as the percentage
730 of total nuclear-associated intensity. Statistical analysis: *** $p < 0.001$, **** $p < 0.0001$.
731
732

733 **Figure 4: Low Ago3 protein level in *squ* mutant triggers Aub–Aub homotypic ping-**
734 **pong**
735 (A) Nucleotide bias of Aub-bound and Ago3-bound piRNAs mapped to piRNA cluster
736 loci in control and *squ* mutant ovaries (replicate 1). Sequence logos indicate 1st to 20th of
737 piRNAs. 10A signature of *squ* mutant condition reflects enhanced Aub–Aub homotypic
738 ping-pong. NA (Not analyzed); Ago3-bound piRNAs are not detectable in *squ* mutant.
739 (B) Nucleotide bias of Aub-bound piRNAs in control and *ago3* mutant ovaries (replicate
740 1).
741 (C) Aub-bound piRNAs from control and *ago3* mutant ovaries mapped to the major
742 germline piRNA clusters *38C-3* and *42AB*. Blue; genomic plus-strand reads, red; minus-
743 strand reads.
744 (D) Antisense bias of Aub-bound piRNAs mapping to transposable elements (TEs) in
745 control and *ago3* mutant ovaries (replicate 1). Each dot represents one TE; antisense
746 piRNA ratios are calculated by dividing antisense-mapping piRNA reads by total
747 mapping reads for each TE. Horizontal lines indicate the mean values. ****$p < 0.0001$
748 (unpaired t-test).
749 (E) Ratio of antisense bias of Aub-bound piRNAs for the 24 up-regulated TEs (detected
750 in *squ* mutant) in *ago3* mutant versus control ovaries (replicate 1). Dots indicate 24 up-
751 regulated TEs (Fig. 2A) in *ago3* mutant relative to control ovaries (replicate 1). For each
752 TE, the antisense bias in *ago3* mutant is divided by that in *ago3* heterozygous.
753
754 **Figure 5: Interaction between Squ and Spn-E is crucial for piRNA biogenesis,**
755 **transposon silencing, and oogenesis**
756 (A) Immunoblotting analysis of Squ interactors in ovaries. Squ is immunoprecipitated
757 from the control *y w* ovaries using anti-Squ antibodies. Precipitation process without anti-
758 Squ antibodies serves as negative control. piRNA biogenesis factors; Spn-E, Tej, Vas,
759 Ago3, and Aub. Ago2, not involved in piRNA biogenesis, serves as a negative control.

760 (B) Immunoprecipitation of GFP–3×Flag–Squ and the variants expressed under the native
761 promoter (pNative-Squ^{WT} and pNative-Squ^{4A}) using anti-3FLAG antibodies. The lower
762 panel shows the quantification of the Squ–Spn-E interaction, plotted as the intensity ratio
763 relative to Squ^{WT} (3 biological replicates).
764 (C) Localization of Squ^{WT} and Squ^{4A} expressed under the native promoter in *squ* mutant
765 germline cells (upper panels: stage 4–5 egg chambers; lower panels: magnified nuclei
766 indicated by squares in the upper panels). Squ^{WT} is enriched in perinuclear nuage, whereas
767 Squ^{4A} shows detached aggregates in the cytoplasm in addition to the perinuclear foci.
768 Scale bar, 5 μm.
769 (D) HCR in situ hybridization of the major germline piRNA precursors derived from
770 clusters *38C* and *42AB* in germline cells of heterozygous control, $squ^{PP32/HE47}$, and
771 $squ^{PP32/HE47}$ expressing Squ^{WT} or Squ^{4A} under the native promoter. DNA is stained with
772 DAPI (blue); the nuclear membrane is labeled with WGA (green). White arrows indicate
773 precursor signals accumulating to perinuclear regions. Scale bar, 2 μm. Right,
774 quantification of perinuclear precursor signals. Fluorescence intensities of foci located
775 within ±5% of the nuclear diameter inside and outside the nuclear membrane are summed,
776 normalized to the total nuclear signal, and plotted as the percentage of perinuclear signal.
777 (E) Immunostaining of HeT-A Gag protein in the heterozygous control,
778 $squ^{PP32/HE47}$mutant, and $squ^{PP32/HE47}$ expressing Squ^{WT} or Squ^{4A} ovaries. Yellow arrows
779 indicate HeT-A Gag signals. Scale bar, 5 μm.
780 (F) RT–qPCR analysis of transcripts derived from the germline-specific transposons
781 *blood*, *HMS-Beagle*, and *Burdock*, with tubulin as a control. All values are normalized to
782 *rp49* and are shown relative to expression levels in $squ^{PP32/HE47}$; pNative-Squ^{WT} ovaries.
783 Error bars indicate standard deviation (3 biological replicates). Statistical significance is
784 assessed by Student's unpaired t-test. *$p < 0.05$, **$p < 0.01$.
785
786 **Figure 6: Squ can stabilize Ago3 without Spn-E**
787 (A) Immunostaining of mid-stage egg chambers from the heterozygous control,

788 *squ*$^{PP32/HE47}$, and *squ*$^{PP32/HE47}$ expressing Squ^{WT} or Squ^{4A} under the native promoter. Scale
789 bar is 5 μm.
790 (B) Immunoblotting of proteins extracted from the heterozygous control, *squ*$^{PP32/HE47}$ and
791 *squ*$^{PP32/HE47}$expressing Squ^{WT} or Squ^{4A} under the native promoter. Lower panel shows the
792 quantification of signal intensities (3 biological replicates). Statistical significance is
793 assessed by Student's unpaired t-test. **p < 0.01.
794 (C) Immunoblotting of proteins extracted from the ovaries of the heterozygous control,
795 *spn-E*$^{7-4}$, and *spn-E*$^{7-4}$ expressing Squ^{WT} or Squ^{4A} under the native promoter. Lower panel
796 shows the quantification of signal intensities (3 biological replicates). Statistical
797 significance is assessed by Student's unpaired t-test. ***p < 0.001, ****p < 0.0001.
798 (D) RT-qPCR measurement of transcripts from piRNA cluster loci, *38C* and *42AB*, those
799 from *HeT-A* and the control tubulin. Relative expression values are obtained by $^{\Delta\Delta}$Ct using
800 *rp49* as reference. Error bars; standard deviation of biological triplicates. Statistics;
801 unpaired T-test (*p <0.05, **p <0.01).
802
803 **Figure 7: The effect of *squ* loss on Spn-E functions**
804 (A) Immunoprecipitation of Aub in the heterozygous control or *squ*$^{PP32/HE47}$ mutant
805 ovaries. Immunoprecipitation without anti-Aub antibodies is shown as a negative control.
806 (B) RT-qPCR measurement of Spn-E-bound piRNA cluster transcripts from *38C* and
807 *42AB*, and the control *tubulin*. RNAs extracted from Spn-E immunoprecipitates from the
808 heterozygous control or *squ*$^{PP32/HE47}$ mutant ovaries are analyzed. Relative values are
809 obtained by $^{\Delta\Delta}$Ct using *rp49* as reference. The signal is further normalized by the Spn-E
810 protein levels in IP fraction (Fig. S7B). Error bars indicate standard deviation (3
811 biological replicates). Beads-only samples are included as a negative control. Statistics;
812 unpaired T-test (*p <0.05).
813 (C) Model for Squ functions in piRNA biogenesis in nuage. Squ contributes through two
814 mechanisms of Squ: (1) Squ directly binds Spn-E, ensuring efficient heterotypic ping-
815 pong between Aub and Ago3 and promoting processing of interacting transcripts

816 including piRNA precursors. (2) Squ stabilizes Ago3 by unknown mechanisms,
817 supporting proper piRNA production. Upon loss of *squ* function, Spn-E remains bound
818 to the Aub* complex at nuage together with the cleaved transcripts which are normally
819 transferred to Ago3. Reduced Ago3 protein is not efficient for proper heterotypic ping-
820 pong, leading a part of Aub to substitute for Ago3 and engage Aub-Aub homotypic ping-
821 pong, which is not effective for piRNA production and TE repression.
822

823 ## Supplemental information

824 **Figure S1: Subcellular localization and expression of Squ in *tej* and *vas* mutants**
825 (A–B) Protein levels and immunostaining of Squ in control ovaries and in *tej* (A) or *vas*
826 (B) mutant egg chambers. Scale bar is 5 μm.
827

828 **Figure S2:**
829 (A) The heatmap of fold changes of TEs' expression for all 119 canonical transposons in
830 control and *squ* mutant ovaries.
831

832 **Figure S3: Second replicate for Aub- and Ago3- bound piRNAs in the control and**
833 ***squ* mutant**
834 (A) Aub- (upper panels) and Ago3-bound (lower panels) small RNAs from control and
835 *squ* mutan ovaries mapped to the major piRNA clusters *38C-3* and *42AB* (replicate 2).
836 Plus-strand (blue) and minus-strand (red) piRNAs are shown as upward and downward
837 peaks, respectively.
838 (B) Antisense bias of Aub-bound piRNAs mapping to transposable elements (TEs) in
839 control (*squ* het) and *squ* mutant ovaries (replicate 2). Each dot represents one TE;
840 antisense piRNA ratios are calculated by dividing antisense-mapping piRNA reads by
841 total mapping reads for each TE. Horizontal lines indicate the mean values. ****$p <$
842 0.0001 (unpaired t-test).

843 (C) Effect of loss of *squ* function on antisense ratio of Aub-bound piRNAs mapping to
844 transposon consensus sequences. Dots indicate 24 up-regulated TEs (Fig. 2A)
845 in *squ* mutant relative to control ovaries (replicate 2). For each TE, the antisense bias
846 in *squ* mutant is divided by that in *squ* heterozygous.
847 (D) RT–qPCR analysis of transcripts derived from major germline piRNA clusters *38C*
848 and *42AB*, with tubulin as a control. All values are normalized to *rp49* and are shown
849 relative to expression levels in the presence of *squ* heterozygous. Error bars indicate
850 standard deviation (3 biological replicates). Statistical significance is assessed by
851 Student's unpaired t-test.
852
853 **Figure S4: Second replicate for Aub-Aub homotypic signature in *squ* and *ago3***
854 **mutants**
855 (A) Nucleotide bias of Aub-bound and Ago3-bound piRNAs mapped to piRNA cluster
856 loci in control and *squ* mutant ovaries (replicate 2). Sequence logos indicate 1st to 20th of
857 piRNAs. 10A signature of *squ* mutant condition reflects enhanced Aub–Aub homotypic
858 ping-pong. NA (Not analyzed); Ago3-bound piRNAs are not detectable in *squ* mutant.
859 (B) Nucleotide bias of Aub-bound piRNAs in control and *ago3* mutant ovaries (replicate
860 2).
861 (C) Aub-bound piRNAs from control and *ago3* mutant ovaries mapped to the major
862 germline piRNA clusters *38C-3* and *42AB*. Blue; genomic plus-strand reads, red; minus-
863 strand reads.
864 (D) Antisense bias of Aub-bound piRNAs mapping to transposable elements (TEs) in
865 control and *ago3* mutant ovaries (replicate 2). Each dot represents one TE; antisense
866 piRNA ratios are calculated by dividing antisense-mapping piRNA reads by total
867 mapping reads for each TE. Horizontal lines indicate the mean values. ****$p < 0.0001$
868 (unpaired t-test).
869 (E) Ratio of antisense bias of Aub-bound piRNAs for the 24 up-regulated TEs (detected
870 in *squ* mutant) in *ago3* mutant versus control ovaries (replicate 2). Dots indicate 24 up-

871 regulated TEs (Fig. 2A) in *ago3* mutant relative to control ovaries (replicate 2). For each
872 TE, the antisense bias in *ago3* mutant is divided by that in *ago3* heterozygous.
873
874 **Figure S5: Interaction of Squ and Spn-E is crucial for *Drosophila* female fertility**
875 (A) Localization of Squ, Ago3 and Krimp in the *squ* heterozygous control germline cells.
876 (upper panels: stage 4–5 egg chambers; lower panels: magnified nuclei indicated by
877 squares in the upper panels). Scale bar is 5 μm.
878 (B) Immunoprecipitation of Myc-tagged Spn-E^{WT} and Spn-E^{4A} using anti-Myc antibodies
879 with the co-expression of Flag-Squ in S2 culture cells. Flag-Squ can be detected in Spn-
880 E^{WT} but not in Spn-E^{4A} immunoprecipitates.
881 (C) Immunoblotting of proteins extracted from the heterozygous control, $squ^{PP32/HE47}$ and
882 $squ^{PP32/HE47}$expressing Squ^{WT} or Squ^{4A} ovaries.
883 (D) RT–qPCR analysis of transcripts derived from major germline piRNA clusters *38C*
884 and *42AB*, with tubulin as a control. All values are normalized to *rp49* and are shown
885 relative to expression levels in $squ^{PP32/HE47}$; pNative-Squ^{WT} ovaries. Error bars indicate
886 standard deviation (3 biological replicates). Statistical significance is assessed by
887 Student's unpaired t-test. *p <0.05.
888 (E) Analysis of egg laying and hatching rate. Infertility of *squ* mutant is rescued by the
889 pNative-promoter-Squ^{WT} but not Squ^{4A} mutant. Daily egg production by five females is
890 recorded (3 biological replicates). T-test is performed for the statistics analysis. (****p
891 <0.0001).
892
893 **Figure S6:**
894 (A) Immunoprecipitation of GFP–3×Flag–Squ and the variants expressed under the
895 native promoter (pNative-Squ^{WT} and pNative-Squ^{4A}) using anti-3FLAG antibodies in the
896 ovaries expressing pNative-Squ^{WT} and - Squ^{4A} under the loss of endogenous *spn-E*
897 condition.
898 (B) Immunoblotting of proteins extracted from the heterozygous control, $squ^{PP32/HE47}$, *squ*

899 heterozygous and *squ*$^{PP32/HE47}$ expressing NGT40; nosGal4 driven Flag-Ago3 protein.
900 Two bands are detected using anti-Ago3 antibodies (upper bands are the NGT40; nosGal4
901 driven Flag-Ago3 and lower bands are the endogenous Ago3).
902
903 **Figure S7: Structural modeling and in vitro characterization of Spn-E and Squ**
904 (A) Quantification of intensity ratio for Aub–Spn-E interaction in the presence and
905 absence of *squ*. Relative values are obtained by $^{\Delta\Delta}$Ct using *rp49* as reference. The signal
906 is further normalized by the Aub protein levels in IP fractions. Error bars indicate standard
907 deviation (3 biological replicates). The beads only controls are also shown as a negative
908 control. Statistics; unpaired T-test.
909 (B) Immunoblotting of the input and Spn-E IP fraction samples in the presence and
910 absence of *squ*. 2, 4, 8 and 16 μl of the IP samples are loaded to perform the comparison
911 of IP efficiency.
912 (C) Predicted structure of the SIWI*/Aub* complex with Spn-E and Squ.
913 (i) Cryo-EM structure of the *Bombyx mori* SIWI/Aub–piRNA–target RNA–GTSF1–
914 Maelstrom–Spn-E complex (PDB: 9NHS). SIWI is shown in gray, GTSF1 in orange,
915 Maelstrom in purple, and Spn-E in dark green. The target RNA is depicted as a cyan
916 ribbon.
917 (ii) Predicted *Drosophila melanogaster* Spn-E–Squ complex generated using AlphaFold3.
918 Spn-E is shown in green and Squ in yellow. A single-stranded RNA is displayed as a blue
919 ribbon, and ATP is shown in stick representation.
920 (iii) Structural superposition of the two models based on alignment of their Spn-E
921 subunits.
922 (D) ATPase activity of purified Spn-E^{WT}, Spn-E^{DQVH}, and Squ. ATP hydrolysis is
923 measured up to 5 h, and released inorganic phosphate is quantified. Spn-E^{WT} shows robust
924 ATPase activity, whereas Spn-E^{DQVH} and Squ alone exhibit minimal ATP hydrolysis.
925 Error bars indicate standard deviation (3 biological replicates). Statistics; unpaired T-test
926 (***$p < 0.001$).

Reference

Adashev VE, Kotov AA, Bazylev SS, Kombarov IA, Olenkina OM, Shatskikh AS, Olenina LV. 2024. Essential functions of RNA helicase Vasa in maintaining germline stem cells and piRNA-guided *Stellate* silencing in *Drosophila* spermatogenesis. *Front Cell Dev Biol*. 12:1450227. doi: 10.3389/fcell.2024.1450227. PMID: 39184915

Anand A, Kai T. 2011. The tudor domain protein kumo is required to assemble the nuage and to generate germline piRNAs in *Drosophila*. *EMBO J*. 31(4):870-882. doi: 10.1038/emboj.2011.449. PMID: 22157814

Andersen PR, Tirian L, Vunjak M, Brennecke J. 2017. A heterochromatin-dependent transcription machinery drives piRNA expression. *Nature*. 549:54-59. doi: 10.1038/nature23482. PMID: 28847004

Andress A, Bei Y, Fonslow BR, Giri R, Wu Y, Yates JR 3rd, Carthew RW. 2016. Spindle-E cycling between nuage and cytoplasm is controlled by Qin and PIWI proteins. *J Cell Biol*. 213:201-211. doi: 10.1083/jcb.201411076. PMID: 27091448

Aravin A, Gaidatzis D, Pfeffer S, Lagos-Quintana M, Landgraf P, Iovino N, Morris P, Brownstein MJ, Kuramochi-Miyagawa S, Nakano T, Chien M, Russo JJ, Ju J, Sheridan R, Sander C, Zavolan M, Tuschl T. 2006. A novel class of small RNAs bind to MILI protein in mouse testes. *Nature*. 442:203-207. doi: 10.1038/nature04916. PMID: 16751777

Aravin AA, Sachidanandam R, Girard A, Fejes-Toth K, Hannon GJ. 2007. Developmentally regulated piRNA clusters implicate MILI in transposon control. *Science*. 316:744-747. doi: 10.1126/science.1142612. PMID: 17446352

Betancourt AJ, Wei KH, Huang Y, Lee YCG. 2024. Causes and Consequences of Varying Transposable Element Activity: An Evolutionary Perspective. *Annu Rev Genomics Hum Genet*. 25:1-25. doi: 10.1146/annurev-genom-120822-105708. PMID: 38603565

954 Brand AH, Perrimon N. 1993. Targeted gene expression as a means of altering cell fates
955 and generating dominant phenotypes. *Development*. 118:401-415. doi:
956 10.1242/dev.118.2.401. PMID: 8223268
957 Brennecke J, Aravin AA, Stark A, Dus M, Kellis M, Sachidanandam R, Hannon GJ. 2007.
958 Discrete small RNA-generating loci as master regulators of transposon activity in
959 *Drosophila*. *Cell*. 128:1089-103. doi: 10.1016/j.cell.2007.01.043. PMID: 17346786
960 Chen S, Zhou Y, Chen Y, Gu J. 2018. fastp: an ultra-fast all-in-one FASTQ preprocessor.
961 *Bioinformatics*. 34:i884-i890. doi: 10.1093/bioinformatics/bty560. PMID:
962 30423086
963 Choi HMT, Schwarzkopf M, Fornace ME, Acharya A, Artavanis G, Stegmaier J, Cunha
964 A, Pierce NA. 2018. Third-generation *in situ* hybridization chain reaction:
965 multiplexed, quantitative, sensitive, versatile, robust. *Development*. 145:dev165753.
966 doi: 10.1242/dev.165753. PMID: 29945988
967 Czech B, Hannon GJ. 2011. Small RNA sorting: matchmaking for Argonautes. *Nat Rev*
968 *Genet*. 12:19-31. doi: 10.1038/nrg2916. PMID: 21116305
969 Darricarrère N, Liu N, Watanabe T, Lin H. 2013. Function of Piwi, a nuclear
970 Piwi/Argonaute protein, is independent of its slicer activity. *Proc Natl Acad Sci U S*
971 *A*. 110:1297-1302. doi: 10.1073/pnas.1213283110. PMID: 23297219
972 De D, Sarkar S, Gebert LFR, Wiryaman T, Anzelon TA, MacRae IJ. 2025. A conserved
973 PIWI silencing complex detects piRNA-target engagement. *Mol Cell*. 85:3275-
974 3287.e7. doi: 10.1016/j.molcel.2025.08.010. PMID: 40912244
975 Dobin A, Davis CA, Schlesinger F, Drenkow J, Zaleski C, Jha S, Batut P, Chaisson M,
976 Gingeras TR. 2012. STAR: ultrafast universal RNA-seq aligner. *Bioinformatics*.
977 29:15-21. doi: 10.1093/bioinformatics/bts635. PMID: 23104886
978 Durdevic Z, Pillai RS, Ephrussi A. 2018. Transposon silencing in the *Drosophila* female
979 germline is essential for genome stability in progeny embryos. *Life Sci Alliance*.
980 1:e201800179. doi: 10.26508/lsa.201800179. PMID: 30456388
981 ElMaghraby MF, Andersen PR, Pühringer F, Hohmann U, Meixner K, Lendl T, Tirian L,

982 Brennecke J. 2019. A Heterochromatin-Specific RNA Export Pathway Facilitates
983 piRNA Production. *Cell*. 178:964-979.e20. doi: 10.1016/j.cell.2019.07.007. PMID:
984 31398345
985 Gokcezade J, Sienski G, Duchek P. 2014. Efficient CRISPR/Cas9 plasmids for rapid and
986 versatile genome editing in *Drosophila*. *G3 (Bethesda)*. 4:2279-2282. doi:
987 10.1534/g3.114.014126. PMID: 25236734
988 Goodier JL, Kazazian HH Jr. 2008. Retrotransposons revisited: the restraint and
989 rehabilitation of parasites. *Cell*. 135:23-35. doi: 10.1016/j.cell.2008.09.022. PMID:
990 18854152
991 Goriaux C, Théron E, Brasset E, Vaury C. 2014. History of the discovery of a master
992 locus producing piRNAs: the flamenco/COM locus in *Drosophila melanogaster*.
993 *Front Genet*. 5:257. doi: 10.3389/fgene.2014.00257. PMID: 25136352
994 Grieder NC, de Cuevas M, Spradling AC. 2000. The fusome organizes the microtubule
995 network during oocyte differentiation in *Drosophila*. *Development*. 127:4253-4264.
996 doi: 10.1242/dev.127.19.4253. PMID: 10976056
997 Gunawardane LS, Saito K, Nishida KM, Miyoshi K, Kawamura Y, Nagami T, Siomi H,
998 Siomi MC. 2007. A slicer-mediated mechanism for repeat-associated siRNA 5' end
999 formation in *Drosophila*. 315:1587-1590. doi: 10.1126/science.1140494. PMID:
1000 17322028
1001 Hedges DJ, Belancio VP. 2011. Restless genomes humans as a model organism for
1002 understanding host-retrotransposable element dynamics. *Adv Genet*. 73:219-262.
1003 doi: 10.1016/B978-0-12-380860-8.00006-9. PMID: 21310298
1004 Hirano T, Iwasaki YW, Lin ZY, Imamura M, Seki NM, Sasaki E, Saito K, Okano H, Siomi
1005 MC, Siomi H. 2014. Small RNA profiling and characterization of piRNA clusters in
1006 the adult testes of the common marmoset, a model primate. *RNA*. 20:1223-1237. doi:
1007 10.1261/rna.045310.114. PMID: 24914035
1008 Jankowsky E, Fairman ME. 2007. RNA helicases--one fold for many functions. *Curr*
1009 *Opin Struct Biol*. 17:316-324. doi: 10.1016/j.sbi.2007.05.007. PMID: 17574830

1010 Jankowsky E. 2011. RNA helicases at work: binding and rearranging. *Trends Biochem*
1011 *Sci*. 36:19-29. doi: 10.1016/j.tibs.2010.07.008. PMID: 20813532
1012 Jeske M, Müller CW, Ephrussi A. 2017. The LOTUS domain is a conserved DEAD-box
1013 RNA helicase regulator essential for the recruitment of Vasa to the germ plasm and
1014 nuage. *Genes Dev*. 31:939-952. doi: 10.1101/gad.297051.117. PMID: 28536148
1015 Kawaguchi S, Xu X, Soga T, Yamaguchi K, Kawasaki R, Shimouchi R, Date S, Kai T.
1016 2025. In silico screening by AlphaFold2 program revealed the potential binding
1017 partners of nuage-localizing proteins and piRNA-related proteins. *Elife*.
1018 13:RP101967. doi: 10.7554/eLife.101967. PMID: 40259744
1019 Kazazian HH Jr. 2004. Mobile elements: drivers of genome evolution. *Science*. 303:1626-
1020 1632. doi: 10.1126/science.1089670. PMID: 15016989
1021 Kina H, Yoshitani T, Hanyu-Nakamura K, Nakamura A. 2019. Rapid and efficient
1022 generation of GFP-knocked-in *Drosophila* by the CRISPR-Cas9-mediated genome
1023 editing. *Dev Growth Differ*. 61:265-275. doi: 10.1111/dgd.12607. PMID: 31037730
1024 Kina H, Izumi N, Hanyu-Nakamura K, Yoshitani T, Yamane M, Niwa H, Tomari Y,
1025 Nakamura A. 2025. Abundant piRNA production mediated by
1026 the *Drosophila* GTSF1 homolog Tpp ensures Aubergine localization and germ
1027 plasm assembly. *Proc Natl Acad Sci U S A*. 122:e2419375122. doi:
1028 10.1073/pnas.2419375122. PMID: 40493187
1029 Kneuss E, Munafò M, Eastwood EL, Deumer US, Preall JB, Hannon GJ, Czech B. 2019.
1030 Specialization of the *Drosophila* nuclear export family protein Nxf3 for piRNA
1031 precursor export. *Genes Dev*. 33:1208-1220. doi: 10.1101/gad.328690.119. PMID:
1032 31416967
1033 Langmead B, Trapnell C, Pop M, Salzberg SL. 2009. Ultrafast and memory-efficient
1034 alignment of short DNA sequences to the human genome. *Genome Biol*. 10:R25. doi:
1035 10.1186/gb-2009-10-3-r25. PMID: 19261174
1036 Li C, Vagin VV, Lee S, Xu J, Ma S, Xi H, Seitz H, Horwich MD, Syrzycka M, Honda
1037 BM, Kittler EL, Zapp ML, Klattenhoff C, Schulz N, Theurkauf WE, Weng Z,

1038 Zamore PD. 2009. Collapse of germline piRNAs in the absence of Argonaute3
1039 reveals somatic piRNAs in flies. *Cell*. 137:509-521. doi: 10.1016/j.cell.2009.04.027.
1040 PMID: 19395009
1041 Liao Y, Smyth GK, Shi W. 2014. featureCounts: an efficient general purpose program for
1042 assigning sequence reads to genomic features. *Bioinformatics*. 30:923-930. doi:
1043 10.1093/bioinformatics/btt656. PMID: 24227677
1044 Lim AK, Kai T. 2007. Unique germ-line organelle, nuage, functions to repress selfish
1045 genetic elements in *Drosophila melanogaster*. *Proc Natl Acad Sci U S A*. 104:6714-
1046 6719. doi: 10.1073/pnas.0701920104. PMID: 17428915
1047 Lim LX, Isshiki W, Iki T, Kawaguchi S, Kai T. 2022. The Tudor Domain-Containing
1048 Protein, Kotsubu (CG9925), Localizes to the Nuage and Functions in piRNA
1049 Biogenesis in *D. melanogaster*. *Front Mol Biosci*. 9:818302. doi:
1050 10.3389/fmolb.2022.818302. PMID: 35425810
1051 Lim RS, Anand A, Nishimiya-Fujisawa C, Kobayashi S, Kai T. 2014. Analysis of Hydra
1052 PIWI proteins and piRNAs uncover early evolutionary origins of the piRNA
1053 pathway. *Dev Biol*. 386:237-251. doi: 10.1016/j.ydbio.2013.12.007. PMID:
1054 24355748
1055 Lim RS, Kai T. 2015. A piece of the pi(e): The diverse roles of animal piRNAs and their
1056 PIWI partners. *Semin Cell Dev Biol*. 47-48:17-31. doi:
1057 10.1016/j.semcdb.2015.10.025. PMID: 26582251.
1058 Lin Y, Suyama R, Kawaguchi S, Iki T, Kai T. 2023. Tejas functions as a core component
1059 in nuage assembly and precursor processing in *Drosophila* piRNA biogenesis. *J Cell*
1060 *Biol*. 222:e202303125. doi: 10.1083/jcb.202303125. PMID: 37555815
1061 Love MI, Huber W, Anders S. 2014. Moderated estimation of fold change and dispersion
1062 for RNA-seq data with DESeq2. *Genome Biol*. 15:550. doi: 10.1186/s13059-014-
1063 0550-8. PMID: 25516281
1064 Lutzmayer S, Enugutti B, Nodine MD. 2017. Novel small RNA spike-in oligonucleotides
1065 enable absolute normalization of small RNA-Seq data. *Sci Rep*. 7:5913. doi:

1066 10.1038/s41598-017-06174-3. PMID: 28724941
1067 Malone CD, Brennecke J, Dus M, Stark A, McCombie WR, Sachidanandam R, Hannon
1068 GJ. 2009. Specialized piRNA pathways act in germline and somatic tissues of the
1069 *Drosophila* ovary. *Cell*. 137:522-535. doi: 10.1016/j.cell.2009.03.040. PMID:
1070 19395010
1071 Malone CD, Hannon GJ. 2009. Small RNAs as guardians of the genome. *Cell*. 136:656-
1072 668. doi: 10.1016/j.cell.2009.01.045. PMID: 19239887
1073 Mendel M, Pillai RS. 2019. Nxf3: a middleman with the right connections for unspliced
1074 piRNA precursor export. *Genes Dev*. 33:1095-1097. doi: 10.1101/gad.330530.119.
1075 PMID: 31481534
1076 Nishida KM, Saito K, Mori T, Kawamura Y, Nagami-Okada T, Inagaki S, Siomi H, Siomi
1077 MC. 2007. Gene silencing mechanisms mediated by Aubergine piRNA complexes
1078 in *Drosophila* male gonad. *RNA*. 13:1911-1922. doi: 10.1261/rna.744307. PMID:
1079 17872506
1080 Ott KM, Nguyen T, Navarro C. 2014. The DExH box helicase domain of spindle-E is
1081 necessary for retrotransposon silencing and axial patterning during *Drosophila*
1082 oogenesis. *G3 (Bethesda)*. 4:2247-2257. doi: 10.1534/g3.114.014332. PMID:
1083 25239103
1084 Pane A, Wehr K, Schüpbach T. 2007. zucchini and squash encode two putative nucleases
1085 required for rasiRNA production in the *Drosophila* germline. *Dev Cell*. 12:851-862.
1086 doi: 10.1016/j.devcel.2007.03.022. PMID: 17543859
1087 Patil VS, Kai T. 2010. Repression of retroelements in *Drosophila* germline via piRNA
1088 pathway by the Tudor domain protein Tejas. *Curr Biol*. 20:724-730. doi:
1089 10.1016/j.cub.2010.02.046. PMID: 20362446
1090 Ramírez F, Bhardwaj V, Arrigoni L, Lam KC, Grüning BA, Villaveces J, Habermann B,
1091 Akhtar A, Manke T. 2018. High-resolution TADs reveal DNA sequences underlying
1092 genome organization in flies. *Nat Commun*. 9:189. doi: 10.1038/s41467-017-02525-
1093 w. PMID: 29335486

1094 Ryazansky SS, Kotov AA, Kibanov MV, Akulenko NV, Korbut AP, Lavrov SA, Gvozdev
1095 VA, Olenina LV. 2016. RNA helicase Spn-E is required to maintain Aub and AGO3
1096 protein levels for piRNA silencing in the germline of *Drosophila*. *Eur J Cell Biol*.
1097 95:311-322. doi: 10.1016/j.ejcb.2016.06.001. PMID: 27320195
1098 Sato K, Iwasaki YW, Shibuya A, Carninci P, Tsuchizawa Y, Ishizu H, Siomi MC, Siomi
1099 H. 2015. Krimper Enforces an Antisense Bias on piRNA Pools by Binding AGO3 in
1100 the *Drosophila* Germline. *Mol Cell*. 59:553-563. doi: 10.1016/j.molcel.2015.06.024.
1101 PMID: 26212455
1102 Schneider CA, Rasband WS, Eliceiri KW. 2012. NIH Image to ImageJ: 25 years of image
1103 analysis. *Nat Methods*. 9:671-675. doi: 10.1038/nmeth.2089. PMID: 22930834
1104 Schüpbach T, Wieschaus E. 1991. Female sterile mutations on the second chromosome
1105 of *Drosophila melanogaster*. II. Mutations blocking oogenesis or altering egg
1106 morphology. *Genetics*. 129:1119-1136. doi: 10.1093/genetics/129.4.1119. PMID:
1107 1783295
1108 Senti KA, Jurczak D, Sachidanandam R, Brennecke J. 2015. piRNA-guided slicing of
1109 transposon transcripts enforces their transcriptional silencing via specifying the
1110 nuclear piRNA repertoire. *Genes Dev*. 29:1747-1762. doi: 10.1101/gad.267252.115.
1111 PMID: 26302790
1112 Shpiz S, Olovnikov I, Sergeeva A, Lavrov S, Abramov Y, Savitsky M, Kalmykova A.
1113 2011. Mechanism of the piRNA-mediated silencing of *Drosophila* telomeric
1114 retrotransposons. *Nucleic Acids Res*. 39:8703-8711. doi: 10.1093/nar/gkr552. PMID:
1115 21764773
1116 Sienski G, Dönertas D, Brennecke J. 2012. Transcriptional silencing of transposons by
1117 Piwi and maelstrom and its impact on chromatin state and gene expression. *Cell*.
1118 151:964-980. doi: 10.1016/j.cell.2012.10.040. PMID: 23159368
1119 Suyama R, Kai T. 2025. piRNA processing within non-membrane structures is governed
1120 by constituent proteins and their functional motifs. *FEBS J*. 292:2715-2736. doi:
1121 10.1111/febs.17360. PMID: 39739617

1122 Wagih O. 2017. ggseqlogo: a versatile R package for drawing sequence logos.
1123 *Bioinformatics*. 33:3645-3647. doi: 10.1093/bioinformatics/btx469. PMID:
1124 29036507.
1125 Wells JN, Feschotte C. 2020. A Field Guide to Eukaryotic Transposable Elements. *Annu*
1126 *Rev Genet*. 54:539-561. doi: 10.1146/annurev-genet-040620-022145. PMID:
1127 32955944
1128 Xiol J, Spinelli P, Laussmann MA, Homolka D, Yang Z, Cora E, Couté Y, Conn S, Kadlec
1129 J, Sachidanandam R, Kaksonen M, Cusack S, Ephrussi A, Pillai RS. 2014. RNA
1130 clamping by Vasa assembles a piRNA amplifier complex on transposon transcripts.
1131 *Cell*. 157:1698-1711. doi: 10.1016/j.cell.2014.05.018. PMID: 24910301
1132 Zhang Z, Xu J, Koppetsch BS, Wang J, Tipping C, Ma S, Weng Z, Theurkauf WE, Zamore
1133 PD. 2011. Heterotypic piRNA Ping-Pong requires qin, a protein with both E3 ligase
1134 and Tudor domains. *Mol Cell*. 44:572-584. doi: 10.1016/j.molcel.2011.10.011.
1135 PMID: 22099305
1136

Figure1:

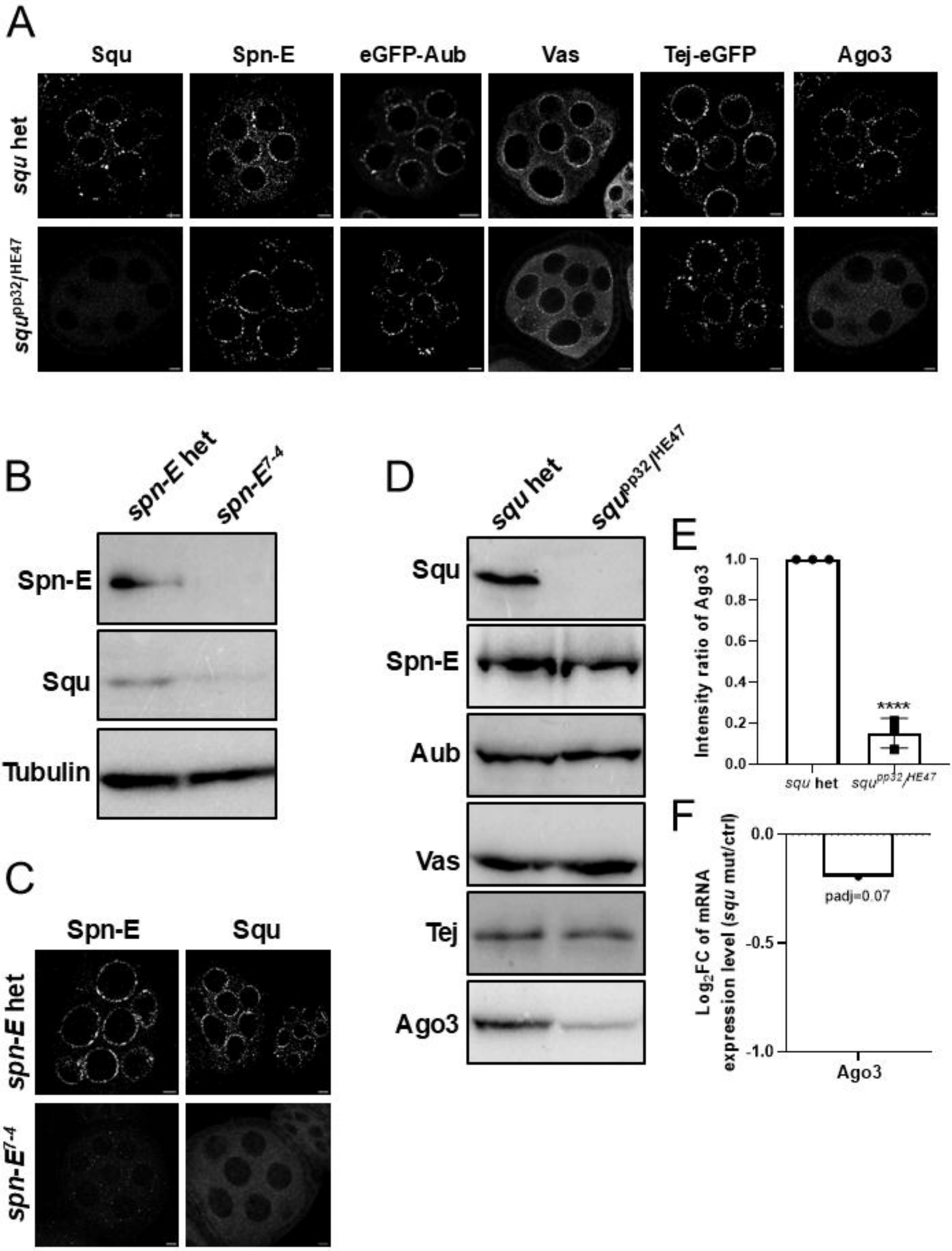
A
Squ
Spn-E
eGFP-Aub
Vas
Tej-eGFP
Ago3
squ het
squpp32/HE47
B
spn-E het
spn-E7-4
Spn-E
Squ
Tubulin
C
Spn-E
Squ
spn-E het
spn-E7-4
D
squ het
squpp32/HE47
Squ
Spn-E
Aub
Vas
Tej
Ago3
E
Intensity ratio of Ago3
1.0
0.8
0.6
0.4
0.2
0.0
****
squ het
squpp32/HE47
F
Log2FC of mRNA expression level (squ mut/ctrl)
0.0
-0.5
-1.0
padj=0.07
Ago3

Figure 2:

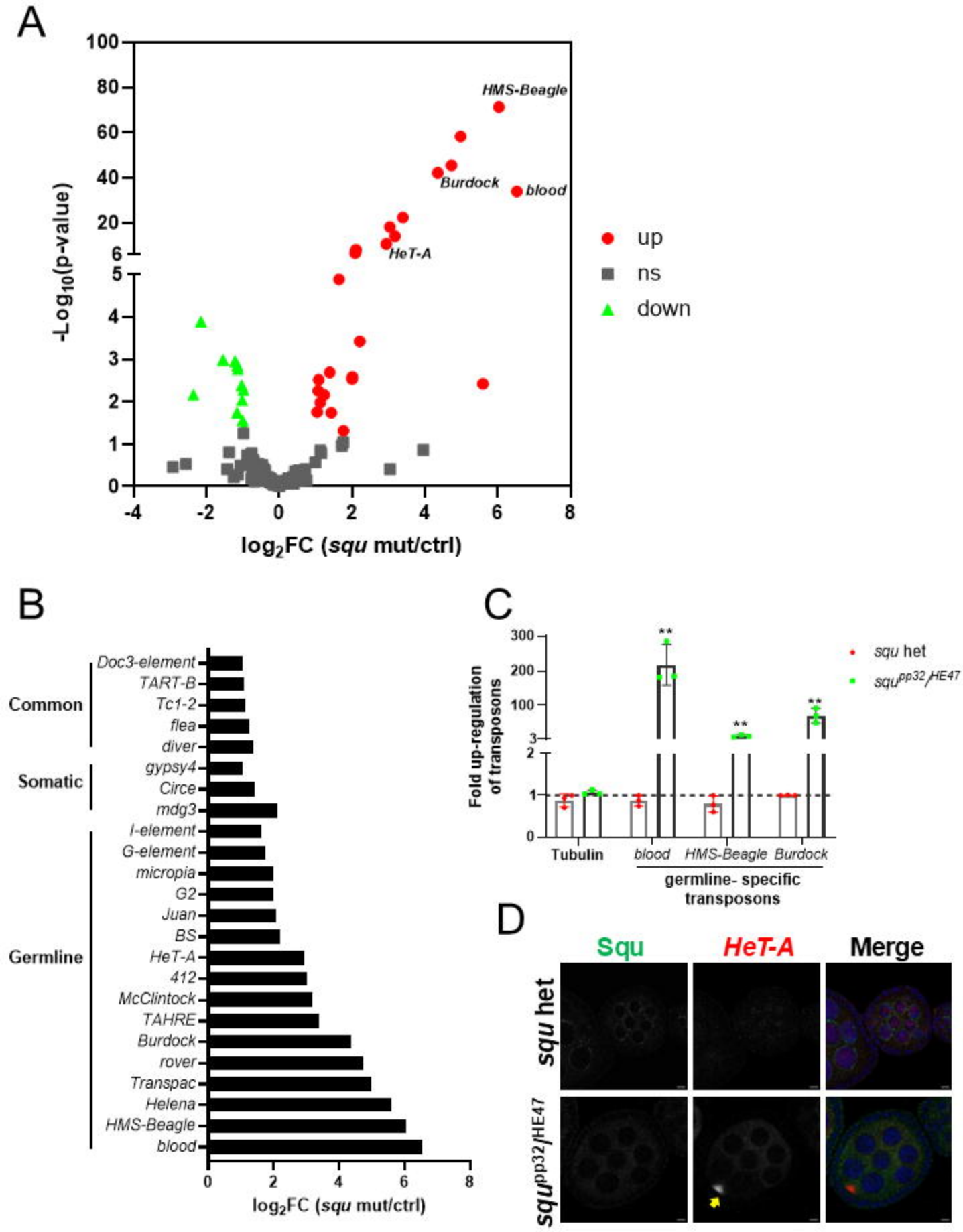
A
HMS-Beagle
Burdock
blood
HeT-A
up
ns
down
-Log10(p-value)
log2FC (squ mut/ctrl)
B
Common
Somatic
Germline
Doc3-element
TART-B
Tc1-2
flea
diver
gypsy4
Circe
mdg3
I-element
G-element
micropia
G2
Juan
BS
HeT-A
412
McClintock
TAHRE
Burdock
rover
Transpac
Helena
HMS-Beagle
blood
log2FC (squ mut/ctrl)
C
squ het
squpp32/HE47
Fold up-regulation of transposons
Tubulin
blood
HMS-Beagle
Burdock
germline- specific transposons
D
Squ
HeT-A
Merge
squ het
squpp32/HE47

Figure 3:

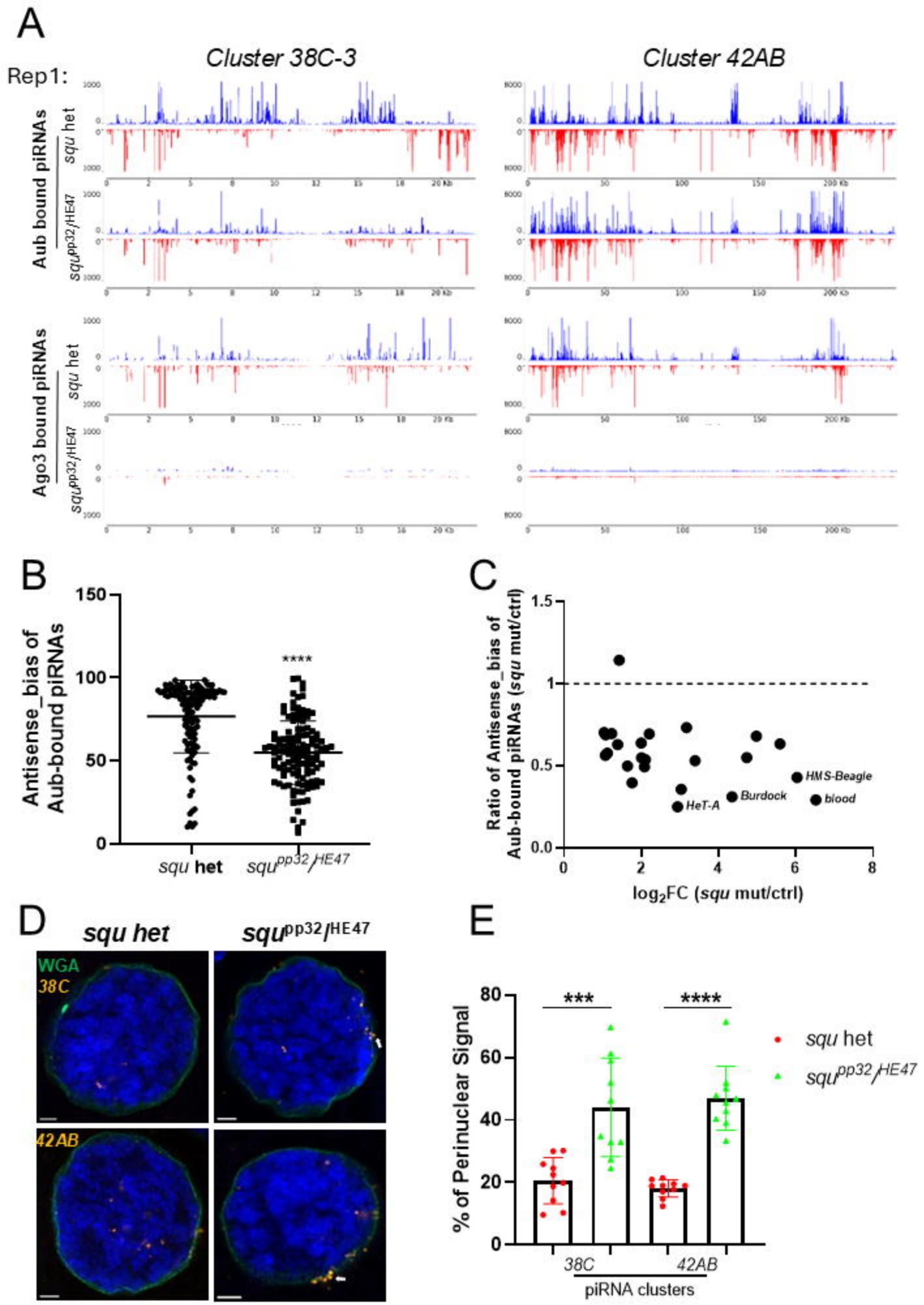
A
Cluster 38C-3
Cluster 42AB
Rep1:
Aub bound piRNAs
Ago3 bound piRNAs
squ het
squpp32/HE47
B
Antisense_bias of Aub-bound piRNAs
****
squ het
squpp32/HE47
C
Ratio of Antisense_bias of Aub-bound piRNAs (squ mut/ctrl)
log2FC (squ mut/ctrl)
HeT-A
Burdock
HMS-Beagle
blood
D
squ het
squpp32/HE47
WGA
38C
42AB
E
% of Perinuclear Signal
***
****
squ het
squpp32/HE47
38C
42AB
piRNA clusters

Figure 4:

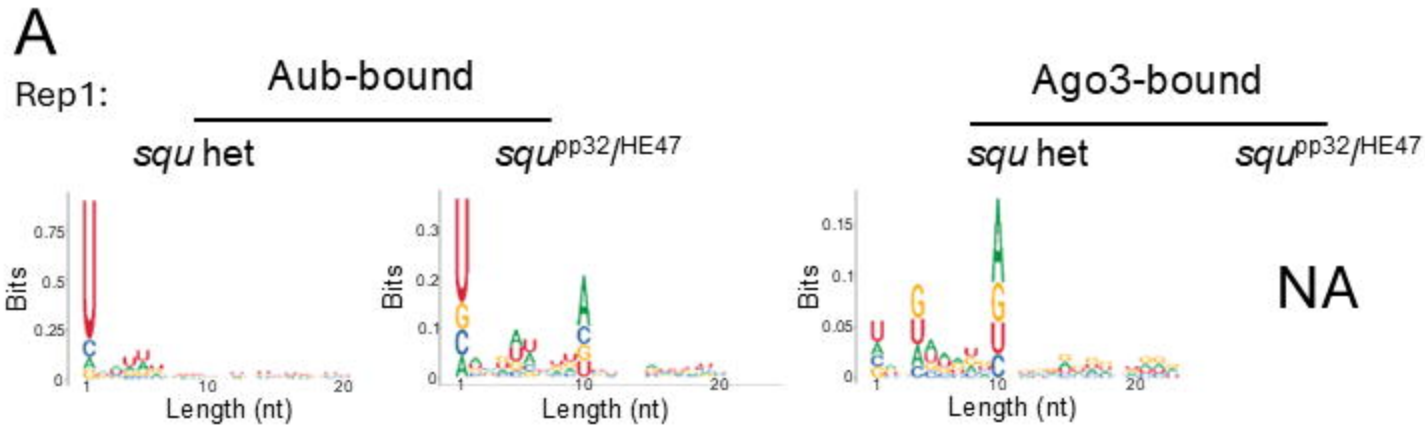
A
Rep1:
Aub-bound
Ago3-bound
squ het
squpp32/HE47
squ het
squpp32/HE47
Bits
Length (nt)
NA

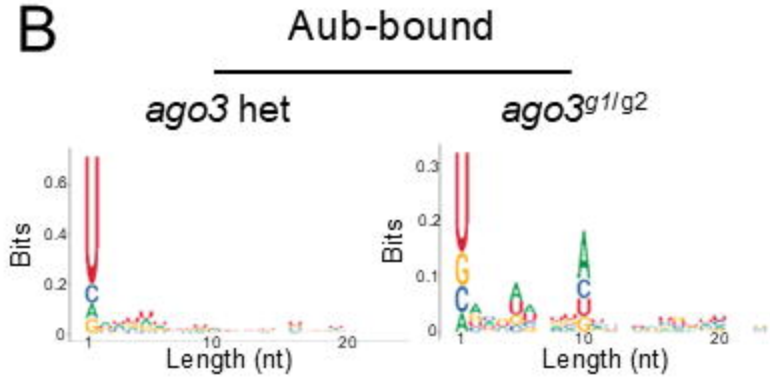
B
Aub-bound
ago3 het
ago3g1/g2
Bits
Length (nt)

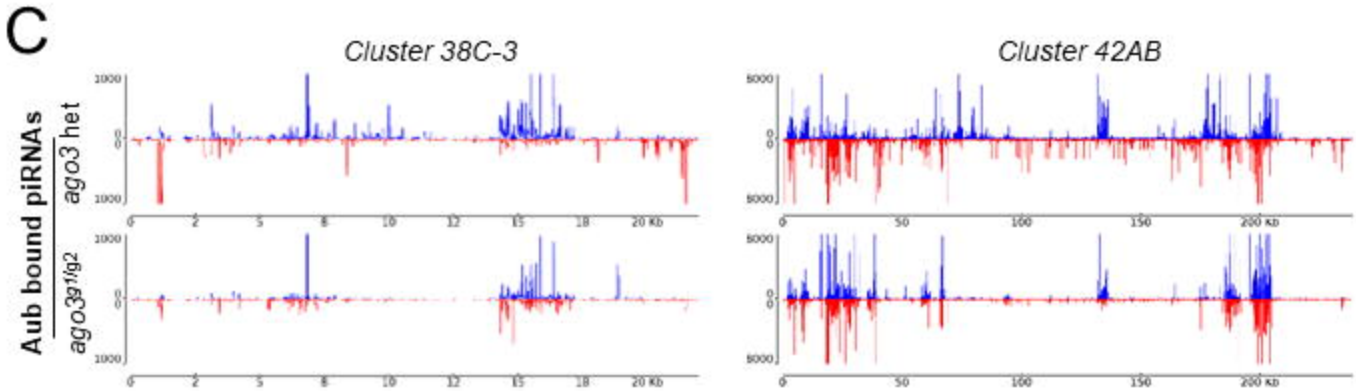
C
Cluster 38C-3
Cluster 42AB
Aub bound piRNAs
ago3 het
ago3g1/g2

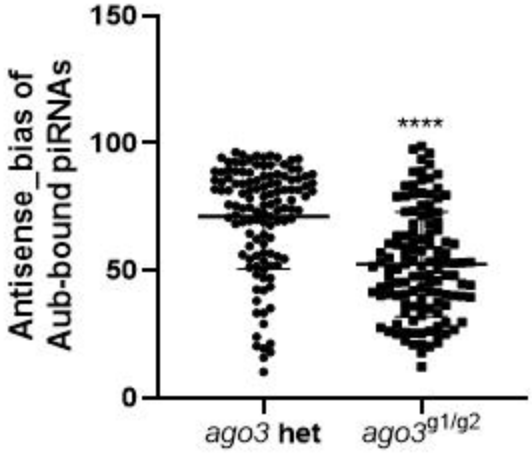
D
Antisense_bias of Aub-bound piRNAs
****
ago3 het
ago3g1/g2

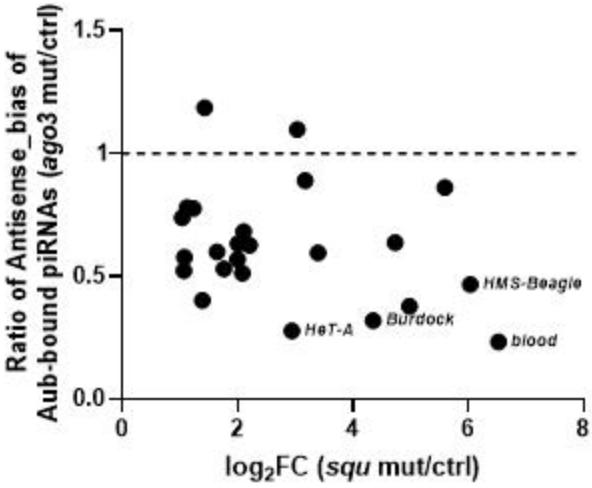
E
Ratio of Antisense_bias of Aub-bound piRNAs (ago3 mut/ctrl)
log2FC (squ mut/ctrl)
HMS-Beagle
HeT-A
Burdock
blood

Figure 5:

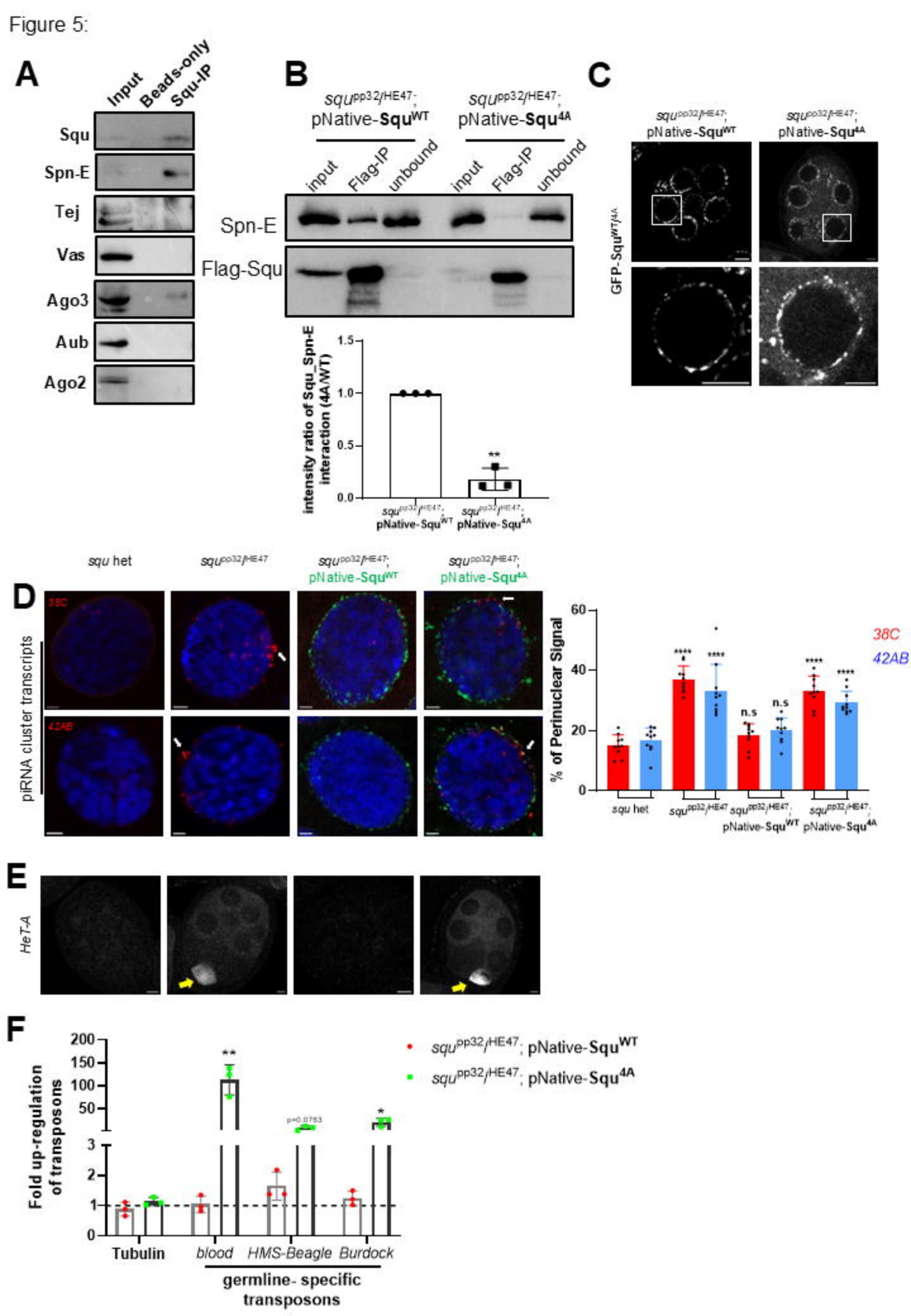
A
Input
Beads-only
Squ-IP
Squ
Spn-E
Tej
Vas
Ago3
Aub
Ago2
B
squpp32/HE47-; pNative-SquWT
squpp32/HE47-; pNative-Squ4A
input
Flag-IP
unbound
Spn-E
Flag-Squ
intensity ratio of Squ_Spn-E interaction (4A/WT)
1.5
1.0
0.5
0.0
**
C
squpp32/HE47-; pNative-SquWT
squpp32/HE47-; pNative-Squ4A
GFP-SquWT/4A
D
squ het
squpp32/HE47
squpp32/HE47-; pNative-SquWT
squpp32/HE47-; pNative-Squ4A
38C
42AB
piRNA cluster transcripts
% of Perinuclear Signal
60
40
20
0
****
n.s
38C
42AB
E
HeT-A
F
Fold up-regulation of transposons
200
150
100
50
3
2
1
0
**
p=0.0763
*
Tubulin
blood
HMS-Beagle
Burdock
germline- specific transposons
squpp32/HE47; pNative-SquWT
squpp32/HE47; pNative-Squ4A

Figure 6:

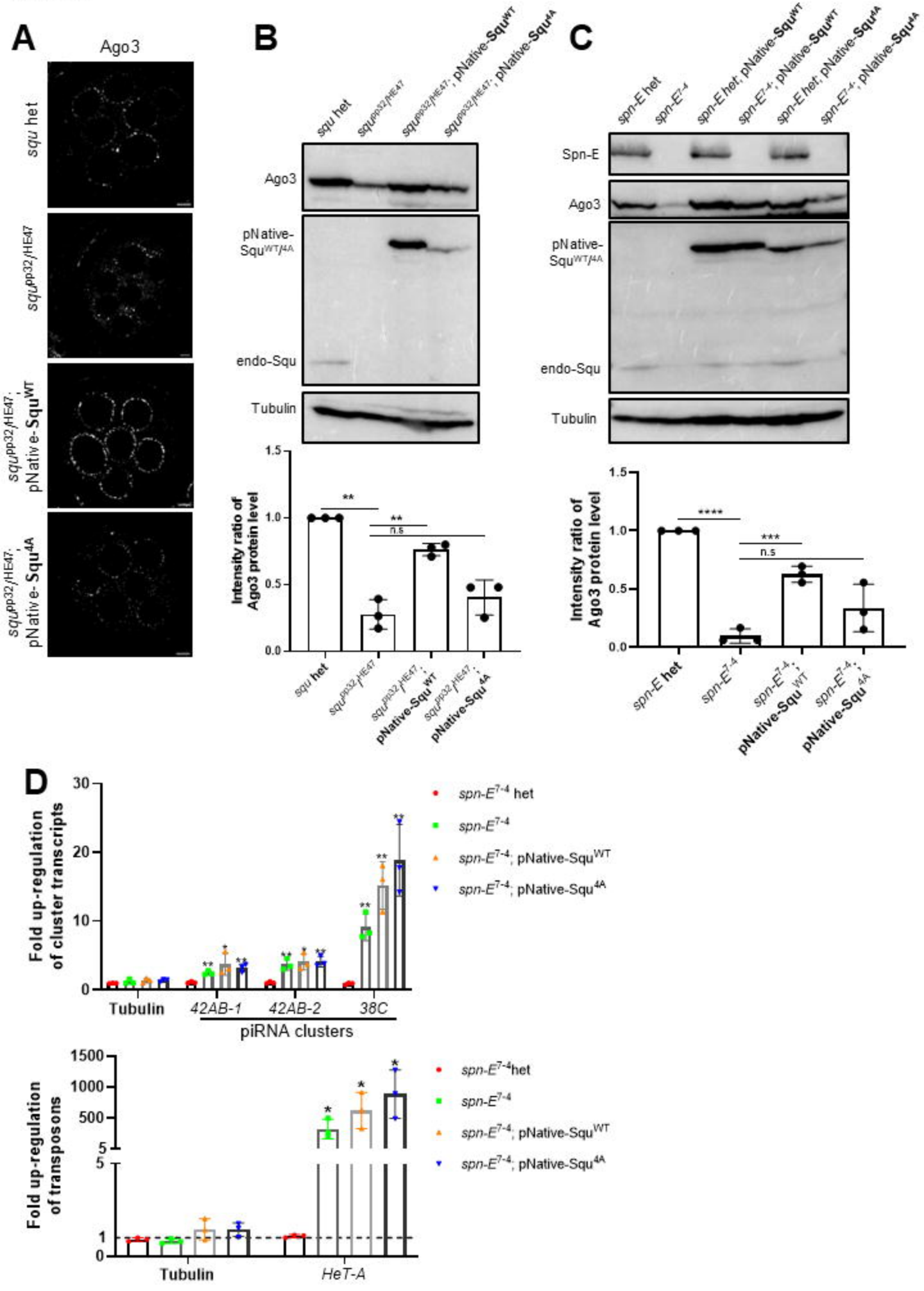
A
Ago3
squ het
squpp32/HE47
squpp32/HE47; pNative-SquWT
squpp32/HE47; pNative-Squ4A
B
squ het
squpp32/HE47
squpp32/HE47; pNative-SquWT
squpp32/HE47; pNative-Squ4A
Ago3
pNative-SquWT/4A
endo-Squ
Tubulin
Intensity ratio of Ago3 protein level
1.5
1.0
0.5
0.0
**
**
n.s
squ het
squpp32/HE47
squpp32/HE47; pNative-SquWT
squpp32/HE47; pNative-Squ4A
C
spn-E het
spn-E7-4
spn-E het; pNative-SquWT
spn-E7-4; pNative-SquWT
spn-E het; pNative-Squ4A
spn-E7-4; pNative-Squ4A
Spn-E
Ago3
pNative-SquWT/4A
endo-Squ
Tubulin
Intensity ratio of Ago3 protein level
1.5
1.0
0.5
0.0
****
***
n.s
spn-E het
spn-E7-4
spn-E7-4; pNative-SquWT
spn-E7-4; pNative-Squ4A
D
Fold up-regulation of cluster transcripts
30
20
10
0
Tubulin
42AB-1
42AB-2
38C
piRNA clusters
spn-E7-4 het
spn-E7-4
spn-E7-4; pNative-SquWT
spn-E7-4; pNative-Squ4A
Fold up-regulation of transposons
1500
1000
500
5
1
0
Tubulin
HeT-A
spn-E7-4 het
spn-E7-4
spn-E7-4; pNative-SquWT
spn-E7-4; pNative-Squ4A

Figure 7:

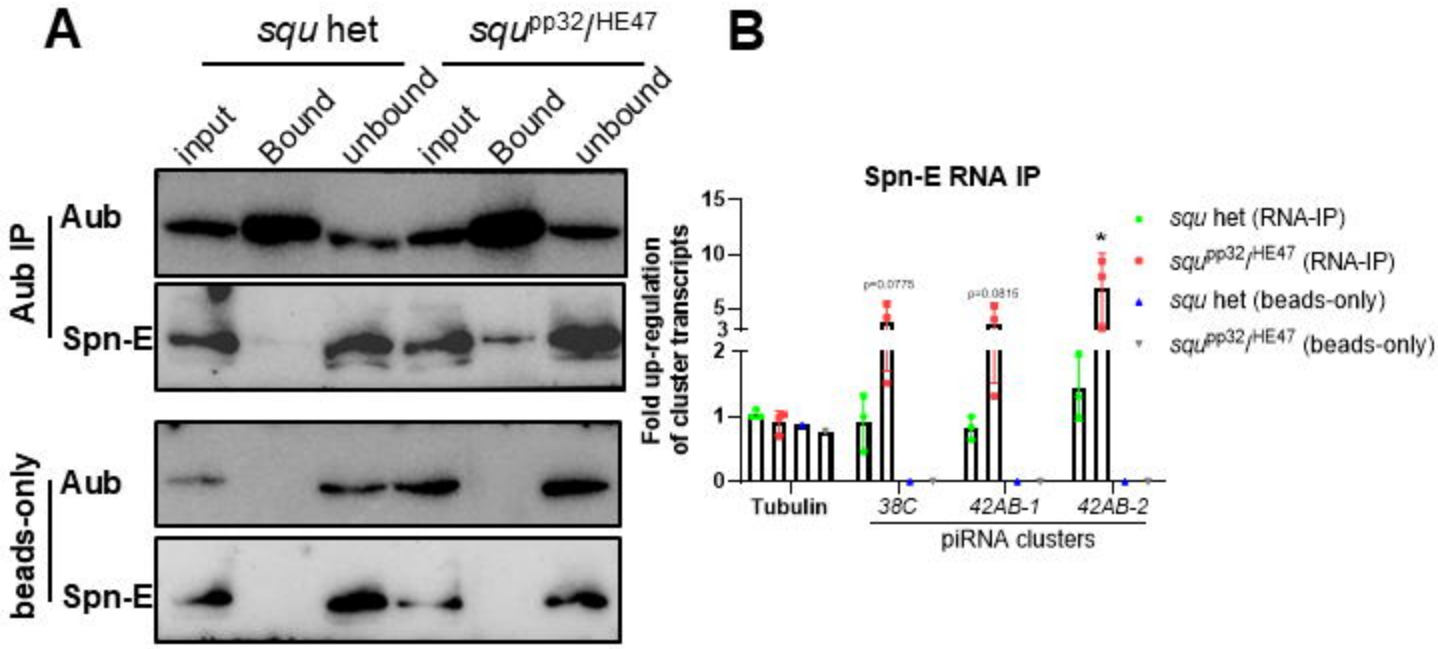
A
squ het
squpp32/HE47
input
Bound
unbound
input
Bound
unbound
Aub IP
Aub
Spn-E
beads-only
Aub
Spn-E
B
Spn-E RNA IP
Fold up-regulation of cluster transcripts
15
10
5
3
2
1
0
p=0.0775
p=0.0815
*
squ het (RNA-IP)
squpp32/HE47 (RNA-IP)
squ het (beads-only)
squpp32/HE47 (beads-only)
Tubulin
38C
42AB-1
42AB-2
piRNA clusters

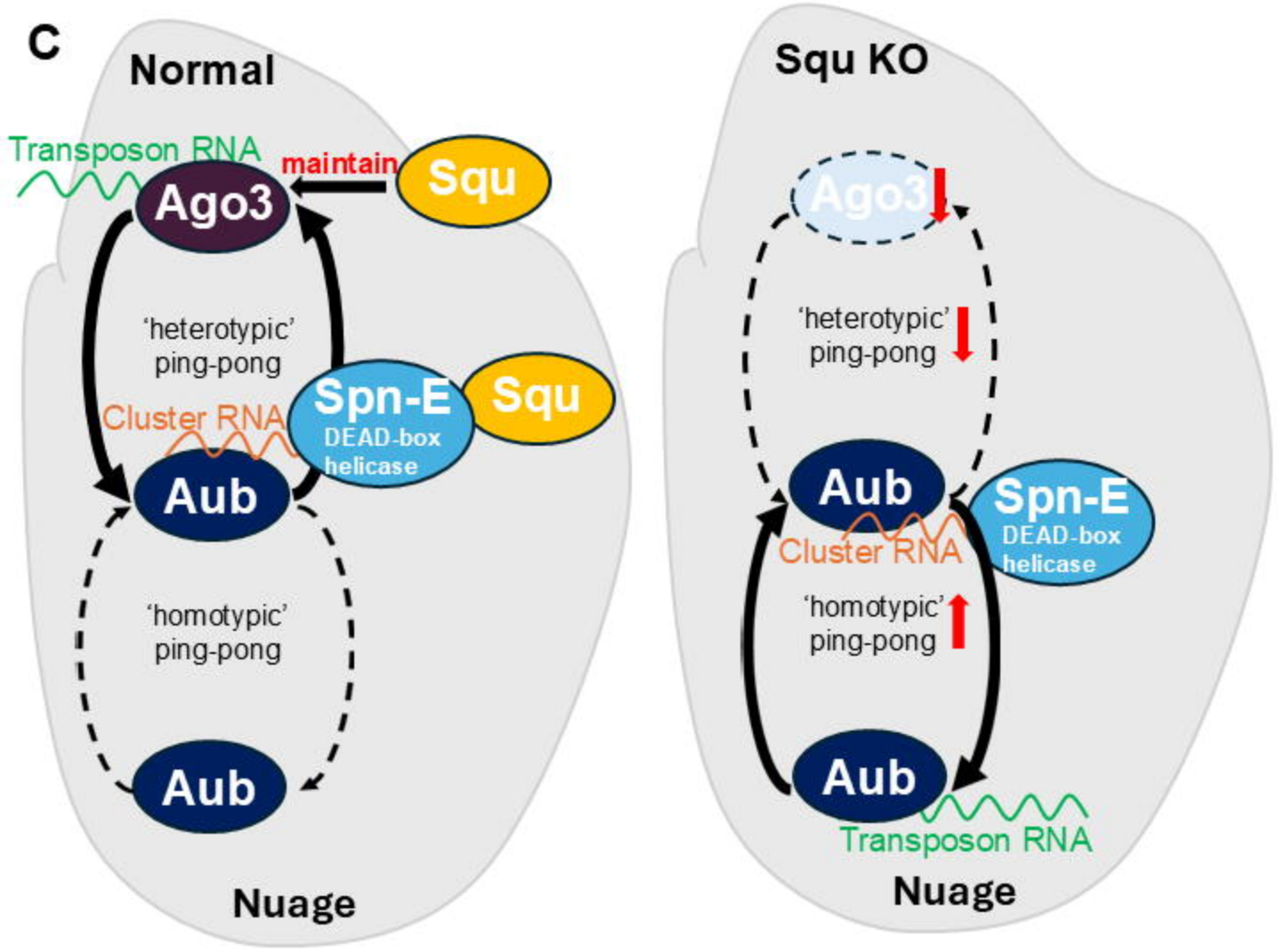
C
Normal
Transposon RNA
maintain
Squ
Ago3
'heterotypic' ping-pong
Cluster RNA
Spn-E
DEAD-box helicase
Squ
Aub
'homotypic' ping-pong
Aub
Nuage
Squ KO
Ago3
'heterotypic' ping-pong
Aub
Spn-E
DEAD-box helicase
Cluster RNA
'homotypic' ping-pong
Aub
Transposon RNA
Nuage